第 43 卷 第 19 期/2023 年 10 月/光学学报 研究论文

光学学报

# 高阶效应下N型量子阱EIT介质中光孤子的存取

胡明君[1]，王登龙[1*]，董耀勇[1,2]，丁建文[1]

[1]湘潭大学物理与光电工程学院，湖南 湘潭 411105；

[2]广东工业大学机电工程学院，广东 广州 510006

**摘要** 构建了由一束弱探测光和两束强控制光耦合到“三明治”型量子阱的能级之间形成N型四能级非对称双量子阱电磁诱导透明(EIT)介质模型，并研究了弱探测光在体系的线性吸收和非线性传播性质。结果表明，当两束控制光均开启后，体系的线性吸收特征曲线呈现出双EIT窗口。有趣的是，无论两束控制光的光强是否相等，所形成的双EIT窗口都呈对称分布。对于非线性情况，仅考虑低阶效应时体系所形成的光孤子并不能稳定地传播而是呈衰减状态；只有计及高阶效应时体系所形成的光孤子才能长距离稳定地传播，且光孤子可通过关闭和开启控制光进行存储和读取。同时还发现，体系所存取的光孤子幅度能通过控制光的光强进行调节。当保持第一控制光的光强不变时，所存取光孤子的幅度随着第二控制光光强的增大而增加；当保持第二控制光的光强不变时，所存取光孤子的幅度随着第一控制光光强的增大而降低。

**关键词** 非线性光学；光孤子的存储与读取；电磁诱导透明；半导体量子阱

**中图分类号** O431；O437 **文献标志码** A **DOI**：10.3788/AOS230630

## 1 引 言

光脉冲因容量大、速度快等优势，被认为是目前量子通信技术中存储信息的最佳载体。然而，在光脉冲传播过程中体系的色散或衍射效应导致传播的波形发生变形，从而引起所传递的信息出现失真[1-3]。光孤子[4-10]是系统的色散(或衍射)效应与系统的非线性效应平衡时产生的稳定的可长距离传播且保持波形不变的光脉冲，因此在传播过程中具有非常高的稳定性[11-16]，可在一定程度上提高量子信息存取的保真度。最初，理论上预言存取光孤子的理想介质是超冷原子电磁诱导透明(EIT)介质[17-18]，这是因为其可以通过弱光激发产生强的非线性光学响应且对光吸收微弱[19-21]，与一般的光脉冲存取相比，光孤子存取的保真度得到大幅度提升[16-18]。Chen等[22]证实在超冷原子EIT介质中可实现两分量至$N$分量的矢量光孤子存取。Shou等[23]发现关闭和开启不同的控制光可将一束携带信号的光孤子在存储后能被两个甚至多个信号源读取。然而，由于超冷原子EIT介质只能在低温下实现，且具有稀薄、不易集成等缺陷，因此很难在具体实际中得到广泛的应用。

随着半导体技术的发展，人们发现半导体固体材料也能传递量子通信中的量子信息[24-26]。这主要是因为半导体量子阱不仅具有与超冷原子相似的分立能级构型，且可在常温下实现，并具有电子数密度高、非线性光学系数大、参数可调、灵活性强、易于小型集成化[27-30]等优势，因此被认为是最有潜力实现EIT应用的介质。Sun等[31]发现选取合适的非对称双量子阱中的失谐量和泵浦场强度，体系会产生强的非线性效应。杜英杰等[32]研究了双量子阱EIT介质中高阶非线性效应对光孤子传输的影响，发现该体系的亮-暗孤子之间的演化取决于群速度色散和三阶非线性系数。随后，人们在推导量子阱体系的非线性薛定谔方程时发现，如果仅考虑低阶效应，体系所形成的光孤子虽然能稳定传播，但受到体系高阶色散及高阶非线性效应的影响，光孤子的波峰随着时间的演化会出现扰动[33]，振幅有所降低，甚至会出现小振幅的色散波[34]。与此同时，Zhu等[35]证实量子阱体系由于能级衰减率较大，形成光孤子所需的探测光脉冲宽度较短，必须使用高阶非线性薛定谔方程[36]所得的孤子解进行数值模拟，体系才能获得稳定传播的光孤子。类似的结果在冷原子[37-38]和半导体量子点体系[39]中也被人们获取。值得一提的是，Tang等[40]发现非对称双量子阱体系在考虑高阶效应后孤子的幅度会出现新奇的现象，即随着纵波光学声子弛豫的增加，孤子的幅度表现为先衰减至最小值再增大。这一系列的研究结果表明，量子阱体

**收稿日期**：2023-03-06；**修回日期**：2023-03-29；**录用日期**：2023-04-23；**网络首发日期**：2023-05-08

**基金项目**：国家自然科学基金(11832016)

**通信作者**：*dlwang@xtu.edu.cn

系可形成光孤子，然而所形成的光孤子能否被量子阱存储和读取？目前对量子阱EIT介质中光孤子的存储和读取的研究报道尚少，尤其是考虑了高阶效应后的光孤子的存储和读取的研究尚未涉及。

本文先构建N型四能级非对称双量子阱EIT介质模型，再研究探测光在体系的线性吸收和非线性传播性质。结果表明，若两束控制光均开启，体系会呈现出双EIT窗口。有趣的是，无论两个控制光强是否相等，双EIT窗口都呈对称分布。非线性情况下，只有考虑高阶效应后所形成的光孤子才能通过控制光的调控被体系存储和读取，且所存储的光孤子幅度可通过控制光强予以调节。这些结果对提高半导体量子阱器件中光信息存储和读取的保真度有一定的参考价值。

## 2　所建模型和麦克斯韦-布洛赫方程组

基于现有的实验条件[41-42]，所构建的N型四能级非对称双量子阱的能级结构[35,43-44]如图1所示。它是由薄势垒分隔的宽阱和窄阱所组成的“三明治”型双量子阱模型，从左往右依次为51单层(145 Å)GaAs宽阱、9单层(25 Å)$Al_{0.2}Ga_{0.8}As$势垒和35单层(100 Å)GaAs窄阱。半导体量子阱介质不仅具有与冷原子相似的能级构型，且可在常温下实现，能在更大范围内调节实际应用过程中所需物理量的各种参数，从而在器件的设计上具有很大的灵活性以及更易于小型集成化，会比相同构型的原子介质具有更高的实用价值[27-30]。能级$|1\rangle$和$|2\rangle$是价带的局域空穴态；能级$|3\rangle$和$|4\rangle$是导带的成键和反键(antibonding)电子态，这是由薄势垒的阱间隧穿效应引起的。中心角频率为$\omega_p$的弱探测光耦合到能级$|1\rangle$和$|3\rangle$之间；中心角频率为$\omega_b$的强控制光耦合到能级$|2\rangle$和$|4\rangle$之间，称为第一控制光；中心角频率为$\omega_c$的强控制光耦合到能级$|2\rangle$和$|3\rangle$之间，称为第二控制光。其中，控制场b和c为嵌套关系的双缀饰场[45-46]。$\Omega_p=(\boldsymbol{e}_p\cdot\boldsymbol{\mu}_{31})E_p/(2\hbar)$为探测光的半拉比频率，两束控制光的半拉比频率分别为$\Omega_b=(\boldsymbol{e}_b\cdot\boldsymbol{\mu}_{42})E_b/(2\hbar)$和$\Omega_c=(\boldsymbol{e}_c\cdot\boldsymbol{\mu}_{32})E_c/(2\hbar)$，其中，$\boldsymbol{\mu}_{31}$、$\boldsymbol{\mu}_{32}$和$\boldsymbol{\mu}_{42}$为相应的带间偶极矩，$\boldsymbol{e}_p$、$\boldsymbol{e}_b$、$\boldsymbol{e}_c$分别为探测光和控制光偏振方向的单位矢量，$E_p$、$E_b$、$E_c$分别为探测光、第一控制光和第二控制光的振幅，$\hbar$为约化普朗克常数。

假设探测光和控制光均沿$z$轴传播，其电场矢量可表示为$\boldsymbol{E}=\sum_{l=p,c,b}\boldsymbol{e}_l\varepsilon_l\exp[\mathrm{i}(\boldsymbol{k}_l\cdot\boldsymbol{z}-\omega_l t)]+\mathrm{c.c.}$，其中$\varepsilon_p$和$\boldsymbol{k}_p$分别为探测光的包络函数及波矢，$\varepsilon_{b(c)}$和$\boldsymbol{k}_{b(c)}$分别为控制光的包络函数及波矢，c.c.表示复共轭。随后，利用半经典理论对N型四能级非对称双量子阱中的光与量子阱相互作用下的性质进行研究，即量子阱用量子力学的哈密顿量来描述，光场则用经典电磁

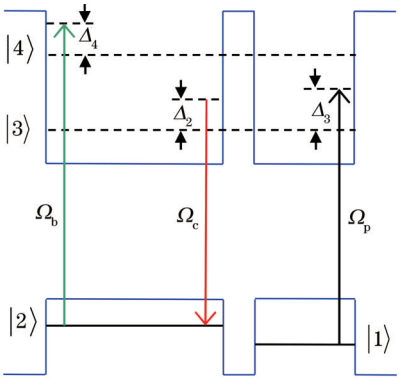


图1　N型四能级非对称双量子阱的能级结构

Fig. 1　Energy-level structure of an N-type four-level asymmetric double quantum well

学理论中的Maxwell方程进行描述。基于电偶极近似和旋转波近似，相互作用绘景下体系的哈密顿量为

$$H_I/\hbar=-\Delta_2|2\rangle\langle 2|-\Delta_3|3\rangle\langle 3|-\Delta_4|4\rangle\langle 4|-\left(\Omega_p|3\rangle\langle 1|-\Delta_c|3\rangle\langle 2|+\Omega_b|4\rangle\langle 2|+\mathrm{h.c.}\right),\tag{1}$$

式中：$\Delta_2=\Delta_p-\Delta_c=\omega_p-\omega_c-\omega_{21}$，$\Delta_3=\Delta_p=\omega_p-\omega_{31}$和$\Delta_4=\Delta_p-\Delta_c+\Delta_b=\omega_b-(\omega_c-\omega_p)-\omega_{41}$分别表示双光子、单光子和三光子失谐量，其中$\Delta_p=\omega_p-\omega_{31}$为探测光的失谐量，$\Delta_{b(c)}=\omega_{b(c)}-\omega_{42(32)}$分别为两束控制光的失谐量，$\omega_{31}$、$\omega_{42}$和$\omega_{32}$为相应能级之间的本征频率；h.c.表示厄米共轭。

在相互作用绘景下，系统的密度矩阵元满足方程$\mathrm{i}\hbar(\partial/\partial t+\Gamma)\hat{\rho}=\left[\hat{H}_I,\hat{\rho}\right]$（$\Gamma$为唯象加入的衰减项，$\hat{\rho}$为密度矩阵，$\hat{H}_I$为相互作用绘景下体系的哈密顿量），从而得到光学Bloch方程

$$\frac{\partial\rho_{11}}{\partial t}=\mathrm{i}\Omega_p^*\rho_{31}-\mathrm{i}\Omega_p\rho_{31}^*+\Gamma_{13}\rho_{33},\tag{2}$$

$$\frac{\partial\rho_{22}}{\partial t}=\mathrm{i}\Omega_c^*\rho_{32}+\mathrm{i}\Omega_b^*\rho_{42}-\mathrm{i}\Omega_c\rho_{32}^*-\mathrm{i}\Omega_b\rho_{42}^*+\Gamma_{23}\rho_{33}+\Gamma_{24}\rho_{44},\tag{3}$$

$$\frac{\partial\rho_{33}}{\partial t}=\mathrm{i}\Omega_p\rho_{31}^*+\mathrm{i}\Omega_c\rho_{32}^*-\mathrm{i}\Omega_p^*\rho_{31}-\mathrm{i}\Omega_c^*\rho_{32}-(\Gamma_{13}+\Gamma_{23})\rho_{33},\tag{4}$$

$$\frac{\partial\rho_{44}}{\partial t}=\mathrm{i}\Omega_b\rho_{42}^*-\mathrm{i}\Omega_b^*\rho_{42}-\Gamma_{24}\rho_{44},\tag{5}$$

$$\frac{\partial\rho_{21}}{\partial t}=\mathrm{i}d_{21}\rho_{21}-\mathrm{i}\Omega_p\rho_{32}^*+\mathrm{i}\Omega_c^*\rho_{31}+\mathrm{i}\Omega_b^*\rho_{41},\tag{6}$$

$$\frac{\partial\rho_{31}}{\partial t}=\mathrm{i}d_{31}\rho_{31}-\mathrm{i}\Omega_p(\rho_{33}-\rho_{11})+\mathrm{i}\Omega_c\rho_{21},\tag{7}$$

$$\frac{\partial\rho_{32}}{\partial t}=\mathrm{i}d_{32}\rho_{32}-\mathrm{i}\Omega_c(\rho_{33}-\rho_{22})+\mathrm{i}\Omega_p\rho_{21}^*-\mathrm{i}\Omega_b\rho_{43}^*,\tag{8}$$

$$\frac{\partial\rho_{41}}{\partial t}=\mathrm{i}d_{41}\rho_{41}+\mathrm{i}\Omega_b\rho_{21}-\mathrm{i}\Omega_p\rho_{43},\tag{9}$$

$$\frac{\partial\rho_{42}}{\partial t}=\mathrm{i}d_{42}\rho_{42}-\mathrm{i}\Omega_b(\rho_{44}-\rho_{22})-\mathrm{i}\Omega_c\rho_{43},\tag{10}$$

$$\frac{\partial\rho_{43}}{\partial t}=\mathrm{i}d_{43}\rho_{43}+\mathrm{i}\Omega_b\rho_{32}^*-\mathrm{i}\Omega_p^*\rho_{41}-\mathrm{i}\Omega_c^*\rho_{42},\tag{11}$$

式中：$d_{21}=\Delta_2+\mathrm{i}\gamma_{21}$；$d_{31}=\Delta_3+\mathrm{i}\gamma_{31}$；$d_{41}=\Delta_4+\mathrm{i}\gamma_{41}$；$d_{32}=(\Delta_3-\Delta_2)+\mathrm{i}\gamma_{32}$；$d_{42}=(\Delta_4-\Delta_2)+\mathrm{i}\gamma_{42}$；$d_{43}=(\Delta_4-\Delta_3)+\mathrm{i}\gamma_{43}$；$\gamma_{ij}=\left(\Gamma_i+\Gamma_j\right)/2+\gamma_{ij}^{(\mathrm{deph})}$为能级$|i\rangle$与$|j\rangle$之间的相干衰减率，其中$\Gamma_j=\sum_{E_i<E_j}\Gamma_{ij}$为自发辐射跃迁引起的退相干衰变率，$\gamma_{ij}^{(\mathrm{deph})}$为界面粗糙程度和声子散射过程引起的退相干变化率，$E_i$、$E_j$分别为系统相应能级的能量值；$\rho_{ij}$为相应的密度矩阵元；上标*表示复共轭。

在慢变包络近似下，探测光的Maxwell方程可写为

$$\mathrm{i}\left(\frac{\partial}{\partial z}+\frac{1}{c}\cdot\frac{\partial}{\partial t}\right)\Omega_\mathrm{p}+k_{13}\rho_{31}=0,\tag{12}$$

式中：$c$为光速；$k_{13}=N\omega_\mathrm{p}\left|\boldsymbol{\mu}_{13}\right|^2/(2\hbar\varepsilon_0 c)$为探测光的传播系数，其中$\varepsilon_0$为真空介电常数，$N$为电子数密度。式(2)～(12)组成了麦克斯韦-布洛赫(M-B)方程组，随后只要求解M-B方程组，就可以获得系统的线性吸收和非线性传播性质。

## 3 光的线性吸收特性

一般情况下，M-B方程组[式(2)～(12)]的精确解难以求取。本文利用多重尺度微扰法[6,19]对其近似求解，设

$$\rho_{ij}=\rho_{ij}^{(0)}+\varepsilon\rho_{ij}^{(1)}+\varepsilon^2\rho_{ij}^{(2)}+\varepsilon^3\rho_{ij}^{(3)}+\varepsilon^4\rho_{ij}^{(4)}+\cdots,\tag{13}$$

$$\Omega_\mathrm{p}=\varepsilon\Omega_\mathrm{p}^{(1)}+\varepsilon^2\Omega_\mathrm{p}^{(2)}+\varepsilon^3\Omega_\mathrm{p}^{(3)}+\varepsilon^4\Omega_\mathrm{p}^{(4)}+\cdots,\tag{14}$$

式中：$\rho_{ij}^{(0)}=\delta_{i1}\delta_{j1}$，其中$\delta_{i1}$、$\delta_{j1}$表示初始时刻相应的电子都布局在基态；$\varepsilon$为与各能态布居衰减相关的特征小参量。各展开项均为多重尺度变量$z_l=\varepsilon^l z(l=0,1,2,3)$、$t_l=\varepsilon^l t(l=0,1)$的函数。将上述展开式代入M-B方程组，可得到关于$\Omega_\mathrm{p}^{(l)}$和$\rho_{ij}^{(l)}$的方程组，即

$$\mathrm{i}\left(\frac{\partial}{\partial z_0}+\frac{1}{c}\cdot\frac{\partial}{\partial t_0}\right)\Omega_\mathrm{p}^{(l)}+k_{13}\rho_{31}^{(l)}=M^{(l)},\tag{15}$$

$$\mathrm{i}\frac{\partial}{\partial t_0}\rho_{11}^{(l)}+\mathrm{i}\Gamma_{13}\left[\rho_{11}^{(l)}+\rho_{22}^{(l)}+\rho_{44}^{(l)}\right]=Y^{(l)},\tag{16}$$

$$\mathrm{i}\frac{\partial}{\partial t_0}\rho_{22}^{(l)}+\Omega_\mathrm{c}^*\rho_{32}^{(l)}-\Omega_\mathrm{c}\rho_{32}^{*(l)}+\Omega_\mathrm{b}^*\rho_{42}^{(l)}-\Omega_\mathrm{b}\rho_{42}^{*(l)}+\mathrm{i}\Gamma_{23}\left[\rho_{11}^{(l)}+\rho_{22}^{(l)}+\rho_{44}^{(l)}\right]-\mathrm{i}\Gamma_{24}\rho_{44}^{(l)}=Z^{(l)},\tag{17}$$

$$\mathrm{i}\frac{\partial}{\partial t_0}\rho_{44}^{(l)}+\Omega_\mathrm{b}\rho_{42}^{*(l)}-\Omega_\mathrm{b}^*\rho_{42}^{(l)}+\mathrm{i}\Gamma_{24}\rho_{44}^{(l)}=B^{(l)},\tag{18}$$

$$\left(\mathrm{i}\frac{\partial}{\partial t_0}+d_{21}\right)\rho_{21}^{(l)}+\Omega_\mathrm{c}^*\rho_{31}^{(l)}+\Omega_\mathrm{b}^*\rho_{41}^{(l)}=N^{(l)},\tag{19}$$

$$\left(\mathrm{i}\frac{\partial}{\partial t_0}+d_{31}\right)\rho_{31}^{(l)}+\Omega_\mathrm{p}^{(l)}+\Omega_\mathrm{c}\rho_{21}^{(l)}=P^{(l)},\tag{20}$$

$$\left(\mathrm{i}\frac{\partial}{\partial t_0}+d_{32}\right)\rho_{32}^{(l)}+\Omega_\mathrm{c}\left[\rho_{11}^{(l)}+2\rho_{22}^{(l)}+\rho_{44}^{(l)}\right]-\Omega_\mathrm{b}\rho_{43}^{*(l)}=Q^{(l)},\tag{21}$$

$$\left(\mathrm{i}\frac{\partial}{\partial t_0}+d_{41}\right)\rho_{41}^{(l)}+\Omega_\mathrm{b}\rho_{21}^{(l)}=H^{(l)},\tag{22}$$

$$\left(\mathrm{i}\frac{\partial}{\partial t_0}+d_{42}\right)\rho_{42}^{(l)}-\Omega_\mathrm{b}\left[\rho_{44}^{(l)}-\rho_{22}^{(l)}\right]-\Omega_\mathrm{c}\rho_{43}^{(l)}=J^{(l)},\tag{23}$$

$$\left(\mathrm{i}\frac{\partial}{\partial t_0}+d_{43}\right)\rho_{43}^{(l)}+\Omega_\mathrm{b}\rho_{32}^{*(l)}-\Omega_\mathrm{c}^*\rho_{42}^{(l)}=G^{(l)},\tag{24}$$

其中$M^{(l)}$、$Y^{(l)}$、$Z^{(l)}$、$B^{(l)}$、$N^{(l)}$、$P^{(l)}$、$Q^{(l)}$、$H^{(l)}$、$J^{(l)}$、$G^{(l)}(l=1,2,3,4)$的表达式见附录A。随后，逐级近似求解方程(15)～(24)，当$l=1$时，得到的一阶近似解为

$$\Omega_\mathrm{p}^{(1)}=F\exp(\mathrm{i}\theta),\tag{25}$$

$$\rho_{31}^{(1)}=\frac{(\omega+d_{21})(\omega+d_{41})-\left|\Omega_\mathrm{b}\right|^2}{D(\omega)}F\exp(\mathrm{i}\theta),\tag{26}$$

$$\rho_{21}^{(1)}=-\frac{(\omega+d_{41})\Omega_\mathrm{c}^*}{D(\omega)}F\exp(\mathrm{i}\theta),\tag{27}$$

$$\rho_{41}^{(1)}=\frac{\Omega_\mathrm{b}\Omega_\mathrm{c}^*}{D(\omega)}F\exp(\mathrm{i}\theta),\tag{28}$$

式中：$D(\omega)=\left|\Omega_\mathrm{b}\right|^2(\omega+d_{31})+\left|\Omega_\mathrm{c}\right|^2(\omega+d_{41})-(\omega+d_{21})(\omega+d_{31})(\omega+d_{41})$，其中$\omega$为中心频率；$F$为慢变量$z_j\left(j=1,2,3\right)$、$t_1$的包络函数；$\theta=K(\omega)z_0-\omega t_0$，其中$K(\omega)$为探测光的线性色散关系。

$$K(\omega)=\frac{\omega}{c}-k_{13}\frac{D_\mathrm{p}}{D(\omega)},\tag{29}$$

式中：$D_\mathrm{p}=\left|\Omega_\mathrm{b}\right|^2-(\omega+d_{21})(\omega+d_{41})$。对式(29)在中心频率$\omega=0$附近进行泰勒展开，有$K(\omega)=K_0+K_1\omega+\frac{1}{2}K_2\omega^2+\frac{1}{6}K_3\omega^3+\cdots$，其中，$K_j=\left[\partial^j K(\omega)/\partial\omega^j\right]\big|_{\omega=0}$，$K_0$的虚部$K_{0\mathrm{i}}$表示介质对探测光的吸收，实部$K_{0\mathrm{r}}$表示介质对探测光的色散。除式(26)～(28)外，其他密度矩阵元$\rho_{ij}^{(1)}=0$。

为了获得系统对探测光的线性吸收特征，分析了在不同$\Omega_\mathrm{b}$和$\Omega_\mathrm{c}$情况下线性吸收$K_{0\mathrm{i}}$随失谐$\Delta_\mathrm{p}$的变化情况，如图2所示。从图2(a)可看出，当两束控制光均关闭时，线性吸收特征曲线在失谐量$\Delta_\mathrm{p}=0$处呈现出洛伦兹吸收峰[图2(a)的实线]，这说明探测光在中心频率处被近共振吸收。这是因为两束控制光均关闭时，从图1所示的能级结构可以看出，N型四能级非对称双量子阱系统被蜕变成二能级系统，探测光在任何二能级传播时都会很大程度被介质吸收[47]。当仅开启第一控制光$\Omega_\mathrm{b}$时，线性吸收特征曲线在失谐量$\Delta_\mathrm{p}=0$处仍然呈现为洛伦兹吸收峰[图2(a)的点划线]，这是因为探测光$\Omega_\mathrm{p}$耦合到能级$|1\rangle$与$|3\rangle$之间，而第一控制光$\Omega_\mathrm{b}$耦合到能级$|2\rangle$与$|4\rangle$之间，这两个耦合通道没有发生能级交叠，导致探测光没有共同的通道，因此在共振处不会产生EIT现象，仍然为洛伦兹线性吸收峰。

接下来，探讨仅开启第二控制光$\Omega_\mathrm{c}$后，系统对探测光的线性吸收性质。图2(b)所示为$\Omega_\mathrm{b}=0$ meV时第二控制光在不同光强下的线性吸收曲线。可以看到，当第二控制光$\Omega_\mathrm{c}=10$ meV时[图2(b)中实线]，原

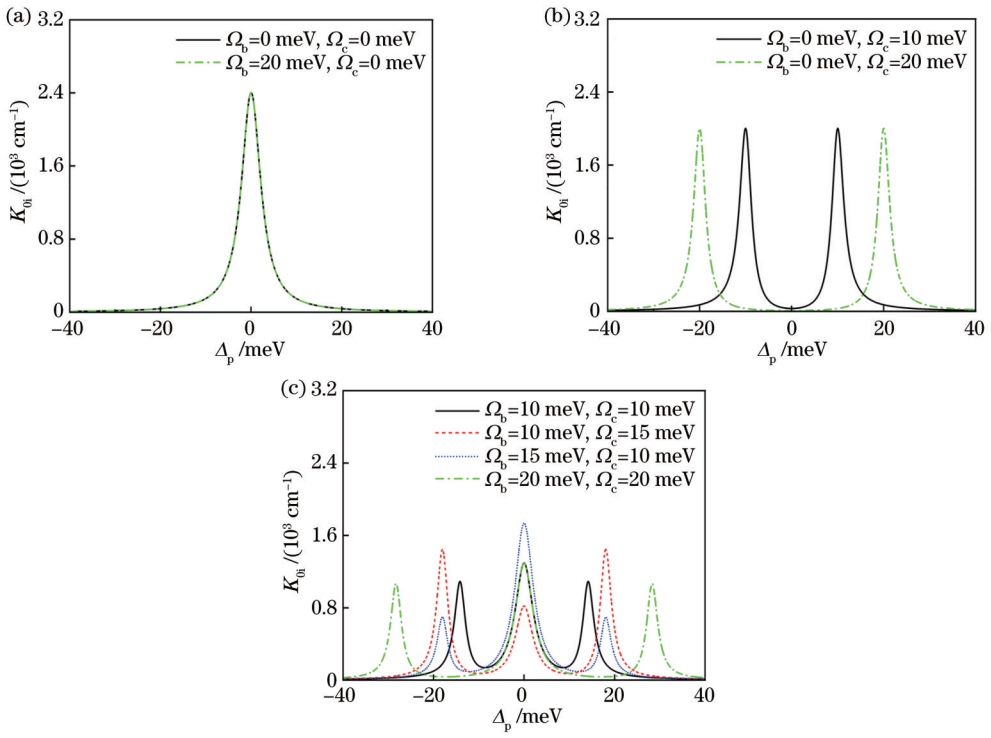


图 2　线性吸收系数 $K_{0i}$ 随着失谐 $\Delta_p$ 的变化情况。(a)关闭第二控制光场 $\Omega_c$;(b)仅开启第二控制光场 $\Omega_c$;(c)控制光场 $\Omega_b$ 和 $\Omega_c$ 均开启

Fig. 2　Linear absorption coefficient $K_{0i}$ as a function of the detuning $\Delta_p$. (a) The second control field $\Omega_c$ is turned off; (b) only the second control field $\Omega_c$ is turned on; (c) both control fields are turned on

来的洛伦兹线性吸收峰发生分裂,出现了单 EIT 窗口。在这种情况下,从图 1 所示的能级结构可以看到,探测光 $\Omega_p$ 耦合到能级$|1\rangle$和$|3\rangle$之间,第二控制光 $\Omega_c$ 耦合到能级$|2\rangle$和$|3\rangle$之间,此时 N 型四能级非对称双量子阱系统蜕化为 Λ 型三能级,强控制光 $\Omega_c$ 诱使两个耦合通道之间产生量子相消干涉效应,从而抑制了介质对探测光的吸收,产生了单 EIT 窗口。当第二控制光增大至 $\Omega_c=20$ meV[图 2(b)中点划线]时,与 $\Omega_c=10$ meV 时的 EIT 窗口宽度相比,此时 EIT 窗口的宽度明显变宽,这说明 EIT 窗口的宽度随着第二控制光强的增加而变宽。

前面仅讨论了开启一束控制光的情况,接着研究两束控制光均开启时系统对探测光的线性吸收性质。图 2(c)所示为不同光强的两束控制光共同作用下的线性吸收曲线。可以看出,当两束控制光都开启且 $\Omega_b=\Omega_c=10$ meV[图 2(c)中实线]时,N 型四能级非对称双量子阱系统出现了双 EIT 窗口。紧接着,保持第一控制光强不变,增大第二控制光强至 $\Omega_c=15$ meV[图 2(c)中短划线],发现透明窗口的宽度变宽了,且左右两窗口呈对称分布。同样地,保持第二控制光为 $\Omega_c=10$ meV,增大第一控制光 $\Omega_b=15$ meV[图 2(c)中短点线],发现透明窗口的宽度变宽了,且两个透明窗口同样呈现对称分布。通过对比图 2(c)中的实线、短划线和短点线,发现:随着任意一个控制光强的增加,透明窗口的宽度都会增大;即使两个控制光强处于不相等的情况下,双 EIT 窗口仍然呈对称分布。当两束控制光同时增大至 $\Omega_b=\Omega_c=20$ meV[图 2(c)中点划线]时,透明窗口的宽度变得更宽了。图 2 中所选参数为 $\gamma_{21}^{(deph)}=\gamma_{31}^{(deph)}=\gamma_{41}^{(deph)}=\gamma_{32}^{(deph)}=\gamma_{42}^{(deph)}=\gamma_{43}^{(deph)}=1/8$ THz，$k_{13}=6.2\times10^5$ m$^{-1}\cdot$meV，$\Gamma_1=\Gamma_2=0$，$\Gamma_3=1$ THz，$\Gamma_4=5/6$ THz，$\Delta_b=\Delta_c=0$。

综上可知:关闭第二控制光时,无论第一控制光如何变化,体系总是呈现洛伦兹线性吸收峰;只有开启第二控制光后体系才会出现 EIT 窗口。若只开启第二控制光(即第一控制光关闭),体系只为单一的 EIT 窗口,窗口的宽度随第二控制光光强的增加而变宽。当两束控制光均开启后,体系会出现双 EIT 窗口,且双 EIT 窗口的宽度随着任意一个控制光强的增加而变宽。有趣的是,不管两个控制光强是否相等,双 EIT 窗口都呈对称分布。

## 4　孤子的稳定性分析

前面探讨了探测光在体系的线性吸收性质,接下来研究其非线性传播性质。当 M-B 方程多重尺度展开至 $l=2$ 时,消除久期项可得

$$\frac{\partial F}{\partial z_1}+\frac{1}{V_g}\cdot\frac{\partial F}{\partial t_1}=0, \tag{30}$$

式中:$V_g=(\partial K/\partial\omega)^{-1}$ 为函数 $F$ 在介质中传播的群速度,可写成 $V_g=V_{gr}+\mathrm{i}V_{gi}$。M-B 方程组的二阶近似解为

$$\Omega_{\mathrm{p}}^{(2)}=0, \tag{31}$$

$$\rho_{31}^{(2)}=\frac{\mathrm{i}}{k_{13}}\left(\frac{1}{V_{\mathrm{g}}}-\frac{1}{c}\right)\frac{\partial F}{\partial t_1}\exp(\mathrm{i}\theta), \tag{32}$$

$$\rho_{21}^{(2)}=\mathrm{i}A_{21}^{(2)}\frac{\partial F}{\partial t_1}\exp(\mathrm{i}\theta), \tag{33}$$

$$\rho_{41}^{(2)}=\mathrm{i}A_{41}^{(2)}\frac{\partial F}{\partial t_1}\exp(\mathrm{i}\theta), \tag{34}$$

$$\rho_{11}^{(2)}=A_{11}^{(2)}|F|^2\exp(-\bar{\alpha}z_2), \tag{35}$$

$$\rho_{22}^{(2)}=A_{22}^{(2)}|F|^2\exp(-\bar{\alpha}z_2), \tag{36}$$

$$\rho_{44}^{(2)}=A_{44}^{(2)}|F|^2\exp(-\bar{\alpha}z_2), \tag{37}$$

$$\rho_{32}^{(2)}=A_{32}^{(2)}|F|^2\exp(-\bar{\alpha}z_2), \tag{38}$$

$$\rho_{42}^{(2)}=A_{42}^{(2)}|F|^2\exp(-\bar{\alpha}z_2), \tag{39}$$

$$\rho_{43}^{(2)}=A_{43}^{(2)}|F|^2\exp(-\bar{\alpha}z_2), \tag{40}$$

式中：$\bar{\alpha}=\varepsilon^{-2}\alpha=2\varepsilon^{-2}\mathrm{Im}[K(\omega)]$，$\alpha$ 表征介质对探测光的吸收；系数 $A_{21}^{(2)}$、$A_{41}^{(2)}$、$A_{11}^{(2)}$、$A_{22}^{(2)}$、$A_{44}^{(2)}$、$A_{32}^{(2)}$、$A_{42}^{(2)}$、$A_{43}^{(2)}$ 的表达式见附录B。

当 $l=3$ 时，消除久期项后可得

$$\mathrm{i}\frac{\partial F}{\partial z_2}-\frac{1}{2}K_2\frac{\partial^2 F}{\partial t_1^2}-W|F|^2F\exp(-\bar{\alpha}z_2)=0, \tag{41}$$

式中：$K_2=\partial^2K/\partial\omega^2$ 为系统的色散系数；$W=-k_{13}J_{\mathrm{w}}/D$ 为系统的克尔非线性系数，$J_{\mathrm{w}}=(\omega+d_{41})\Omega_{\mathrm{c}}A_{32}^{*(2)}-D_{\mathrm{p}}\left[2A_{11}^{(2)}+A_{22}^{(2)}+A_{44}^{(2)}\right]-\Omega_{\mathrm{b}}^{*}\Omega_{\mathrm{c}}A_{43}^{(2)}$，$D=|\Omega_{\mathrm{b}}|^2(\omega+d_{31})+|\Omega_{\mathrm{c}}|^2(\omega+d_{41})-(\omega+d_{21})(\omega+d_{31})(\omega+d_{41})$。M-B方程组的三阶近似解为

$$\Omega_{\mathrm{p}}^{(3)}=0, \tag{42}$$

$$\rho_{31}^{(3)}=\left[A_{31'}^{(3)}\frac{\partial^2F}{\partial t_1^2}+A_{31''}^{(3)}\exp(-\bar{\alpha}z_2)|F|^2F\right]\exp(\mathrm{i}\theta), \tag{43}$$

$$\rho_{21}^{(3)}=\left[A_{21'}^{(3)}\frac{\partial^2F}{\partial t_1^2}+A_{21''}^{(3)}\exp(-\bar{\alpha}z_2)|F|^2F\right]\exp(\mathrm{i}\theta), \tag{44}$$

$$\rho_{41}^{(3)}=\left[A_{41'}^{(3)}\frac{\partial^2F}{\partial t_1^2}+A_{41''}^{(3)}\exp(-\bar{\alpha}z_2)|F|^2F\right]\exp(\mathrm{i}\theta), \tag{45}$$

$$\rho_{11}^{(3)}=\mathrm{i}\left[A_{11'}^{(3)}F^*\frac{\partial F}{\partial t_1}-A_{11''}^{(3)}F\frac{\partial F^*}{\partial t_1}\right]\exp(-\bar{\alpha}z_2), \tag{46}$$

$$\rho_{22}^{(3)}=\mathrm{i}\left[A_{22'}^{(3)}F^*\frac{\partial F}{\partial t_1}-A_{22''}^{(3)}F\frac{\partial F^*}{\partial t_1}\right]\exp(-\bar{\alpha}z_2), \tag{47}$$

$$\rho_{44}^{(3)}=\mathrm{i}\left[A_{44'}^{(3)}F^*\frac{\partial F}{\partial t_1}-A_{44''}^{(3)}F\frac{\partial F^*}{\partial t_1}\right]\exp(-\bar{\alpha}z_2), \tag{48}$$

$$\rho_{32}^{(3)}=\mathrm{i}\left[A_{32'}^{(3)}F^*\frac{\partial F}{\partial t_1}-A_{32''}^{(3)}F\frac{\partial F^*}{\partial t_1}\right]\exp(-\bar{\alpha}z_2), \tag{49}$$

$$\rho_{42}^{(3)}=\mathrm{i}\left[A_{42'}^{(3)}F^*\frac{\partial F}{\partial t_1}-A_{42''}^{(3)}F\frac{\partial F^*}{\partial t_1}\right]\exp(-\bar{\alpha}z_2), \tag{50}$$

$$\rho_{43}^{(3)}=\mathrm{i}\left[A_{43'}^{(3)}F^*\frac{\partial F}{\partial t_1}-A_{43''}^{(3)}F\frac{\partial F^*}{\partial t_1}\right]\exp(-\bar{\alpha}z_2), \tag{51}$$

系数 $A_{31'}^{(3)}$、$A_{31''}^{(3)}$、$A_{21'}^{(3)}$、$A_{21''}^{(3)}$、$A_{41'}^{(3)}$、$A_{41''}^{(3)}$、$A_{11'}^{(3)}$、$A_{11''}^{(3)}$、$A_{22'}^{(3)}$、$A_{22''}^{(3)}$、$A_{44'}^{(3)}$、$A_{44''}^{(3)}$、$A_{32'}^{(3)}$、$A_{32''}^{(3)}$、$A_{42'}^{(3)}$、$A_{42''}^{(3)}$、$A_{43'}^{(3)}$、$A_{43''}^{(3)}$ 的表达式见附录C。

结合式(30)和式(41)并返回到原变量，可以得到非线性薛定谔方程

$$\mathrm{i}\left(\frac{\partial}{\partial z}+\alpha\right)U-\frac{K_2}{2}\cdot\frac{\partial^2U}{\partial\tau^2}-W|U|^2U=0, \tag{52}$$

式中：$\tau=t-z/V_{\mathrm{g}}$；$U=\varepsilon F\exp(-\bar{\alpha}z_2)$。为了简化式(52)，可在EIT窗口中选取合适的参数。根据文献[35,48-51]，半导体量子阱EIT介质中的各参数可选为 $\gamma_{21}^{(\mathrm{deph})}=\gamma_{31}^{(\mathrm{deph})}=\gamma_{41}^{(\mathrm{deph})}=\gamma_{32}^{(\mathrm{deph})}=\gamma_{42}^{(\mathrm{deph})}=\gamma_{43}^{(\mathrm{deph})}=1/8$ THz、$k_{13}=6.2\times10^5\ \mathrm{m^{-1}\cdot meV}$、$\Gamma_1=\Gamma_2=0$、$\Gamma_3=1$ THz、$\Gamma_4=5/6$ THz、$\Delta_{\mathrm{b}}=5.5\times10^{13}\ \mathrm{s^{-1}}$、$\Delta_{\mathrm{c}}=5\times10^{13}\ \mathrm{s^{-1}}$，当 $\Omega_{\mathrm{b}}=8\times10^{13}\ \mathrm{s^{-1}}$、$\Omega_{\mathrm{c}}=24\times10^{13}\ \mathrm{s^{-1}}$ 且 $\Delta_{\mathrm{p}}=5.015\times10^{13}\ \mathrm{s^{-1}}$ 时，可得到 $K_0=(-2.74+\mathrm{i}3.96\times10^{-2})\ \mu\mathrm{m^{-1}}$、$K_1=(7.50\times10^{-14}-\mathrm{i}1.02\times10^{-15})\ \mu\mathrm{m^{-1}\cdot s}$、$K_2=(-1.82\times10^{-27}+\mathrm{i}5.67\times10^{-29})\ \mu\mathrm{m^{-1}\cdot s^2}$、$W=(-7.22\times10^{-28}+\mathrm{i}8.99\times10^{-30})\ \mu\mathrm{m^{-1}\cdot s^2}$。同时也计算出 $\alpha\ll1$，这是因为参数 $\alpha$ 表征系统对探测光的吸收，在EIT窗口内 $\alpha\approx0$。从上述 $K_2$（可写成 $K_2=K_{2\mathrm{r}}+\mathrm{i}K_{2\mathrm{i}}$）和 $W$（可写成 $W=W_{2\mathrm{r}}+\mathrm{i}W_{2\mathrm{i}}$）的表达式可以得出，它们的实部远大于虚部，即 $|K_{2\mathrm{r}}|\gg|K_{2\mathrm{i}}|$ 和 $|W_{\mathrm{r}}|\gg|W_{\mathrm{i}}|$，从而式(52)中的系数 $K_2$ 和 $W$ 可分别用它们的实部 $K_{2\mathrm{r}}$ 和 $W_{\mathrm{r}}$ 表示。随后，引入无量纲参数 $s=-z/(2L_{\mathrm{D}})$、$\sigma=\tau/\tau_0$、$u=U/U_0$，其中 $L_{\mathrm{D}}=\tau_0^2/K_{2\mathrm{r}}$ 为特征色散长度，$\tau_0=1\times10^{-13}$ s为探测光的特征时间长度，$U_0$ 为探测光的半拉比频率。当体系中色散效应和非线性效应平衡时，即 $L_{\mathrm{D}}=L_{\mathrm{NL}}$，可得到 $U_0=(1/\tau_0)\sqrt{K_{2\mathrm{r}}/W_{\mathrm{r}}}$，非线性长度 $L_{\mathrm{NL}}=1/(U_0^2W_{\mathrm{r}})$。式(52)可写为

$$\mathrm{i}\frac{\partial u}{\partial s}+\frac{\partial^2u}{\partial\sigma^2}+2|u|^2u=0。 \tag{53}$$

通过求解式(53)，再返回原始变量，得到考虑低阶效应时的基本孤子解[16]为

$$\Omega_{\mathrm{p}}(z,t)=\frac{1}{\tau_0}\sqrt{\frac{K_{2\mathrm{r}}}{W_{\mathrm{r}}}}\,\mathrm{sech}\left[\frac{1}{\tau_0}\left(t-\frac{z}{V_{\mathrm{gr}}}\right)\right]\exp\left(\mathrm{i}K_{0\mathrm{r}}z-\mathrm{i}\frac{z}{2L_{\mathrm{D}}}\right)。 \tag{54}$$

随后探究体系在考虑低阶效应时所形成的光孤子的稳定性。图3所示为孤子解[式(54)]所描述的探测光光强的幅度 $\left|\Omega_{\mathrm{p}}/U_0\right|^2$ 随时间 $t$ 演化的情况。图3中实线、短划线、短点线、点划线分别表示初始状态以及演化0.5、1.0和1.5个单位长度时的数值结果。可以看出，随着时间的演化，光孤子向右传播：当孤子传播至 $z/(2L_{\mathrm{D}})=0.5$ 处（图3中短划线）时，光孤子的振幅已出现稍微衰减的现象；当光孤子继续向右传播至

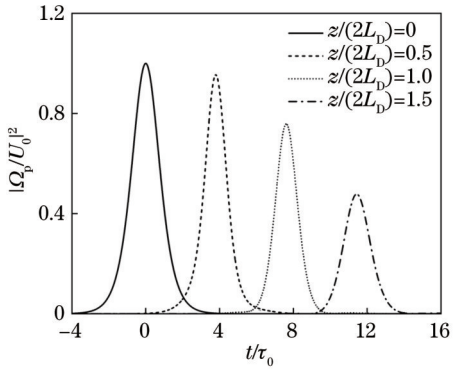


图 3　考虑低阶效应时的光孤子稳定性分析

Fig. 3　Stability analysis of optical soliton considering low-order effect

$z/(2L_D)=1.0$ 处(图 3 中短点线)时,孤子的振幅明显衰减;当光孤子进一步往右传播至 $z/(2L_D)=1.5$ 处(图 3 中点划线)时,光孤子的振幅衰减得更多,这说明此种情况下所形成的光孤子不能长距离稳定地传播,这一光孤子的不稳定性是由系统的高阶色散引起的[34]。图 3 中所用的参数为 $\tau_0=1\times10^{-13}$ s、$\Delta_b=5.5\times10^{13}\ s^{-1}$、$\Delta_c=5\times10^{13}\ s^{-1}$、$\Delta_p=5.015\times10^{13}\ s^{-1}$,其他参数与图 2 相同。

由于考虑低阶效应时所形成的光孤子不能在 N 型四能级非对称双量子阱系统中稳定地传播,因此探究体系计及高阶效应时所形成的光孤子的稳定性。将 M-B 方程多重尺度渐近展开至 $l=4$,消除久期项后得到

$$\mathrm{i}\frac{\partial F}{\partial z_3}-\mathrm{i}\frac{K_3}{6}\cdot\frac{\partial^3 F}{\partial t_1^3}-\mathrm{i}\beta_1\exp(-\bar{\alpha}z_2)\frac{\partial}{\partial t_1}\left(|F|^2F\right)+\mathrm{i}\beta_2\exp(-\bar{\alpha}z_2)F\frac{\partial}{\partial t_1}\left(|F|^2\right)=0,\tag{55}$$

式中:$K_3$、$\beta_1$ 和 $\beta_2$ 分别为系统的三阶色散、非线性色散和非线性折射率延迟效应。

$$K_3=\frac{3k_{13}(2\omega+d_{21}+d_{41})(6\omega+2d_{21}+2d_{31}+2d_{41})-6k_{13}D_x-6k_{13}D_p}{D^2}+\frac{6k_{13}D_pD_x^3}{D^4}+\frac{6k_{13}(2\omega+d_{21}+d_{41})D_x^2+6k_{13}D_xD_p(6\omega+2d_{21}+2d_{31}+2d_{41})}{D^3},\tag{56}$$

$$\beta_1=\frac{k_{13}(\omega+d_{41})\Omega_c}{D}\left[A_{21''}^{(3)}-A_{32'}^{*(3)}-A_{32''}^{*(3)}\right]+\frac{k_{13}D_p}{D}\left\{\left[2A_{11'}^{(3)}+A_{22'}^{(3)}+A_{44'}^{(3)}\right]+\left[2A_{11''}^{(3)}+A_{22''}^{(3)}+A_{44''}^{(3)}\right]+A_{31''}^{(3)}\right\}+\frac{k_{13}\Omega_b^*\Omega_c}{D}\left[A_{43'}^{(3)}+A_{43''}^{(3)}-A_{41''}^{(3)}\right],\tag{57}$$

$$\beta_2=\frac{k_{13}D_p}{D}\left\{\left[2A_{11'}^{(3)}+A_{22'}^{(3)}+A_{44'}^{(3)}\right]+2\left[2A_{11''}^{(3)}+A_{22''}^{(3)}+A_{44''}^{(3)}\right]\right\}-\frac{k_{13}(\omega+d_{41})\Omega_c}{D}\left[A_{32'}^{(3)}+2A_{32''}^{(3)}\right]+\frac{k_{13}\Omega_b^*\Omega_c}{D}\left[A_{43'}^{(3)}+2A_{43''}^{(3)}\right],\tag{58}$$

$$D_x=|\Omega_b|^2+|\Omega_c|^2-(\omega+d_{21})(\omega+d_{31})-(\omega+d_{21})(\omega+d_{41})-(\omega+d_{31})(\omega+d_{41})。\tag{59}$$

结合式(30)、(41)、(55)并返回到初始变量后,可以得到一个复系数的高阶非线性薛定谔方程:

$$\mathrm{i}\frac{\partial U}{\partial z}+\mathrm{i}\frac{\alpha}{2}U-\frac{K_2}{2}\cdot\frac{\partial^2U}{\partial\tau^2}-\mathrm{i}\frac{K_3}{6}\cdot\frac{\partial^3U}{\partial\tau^3}-W|U|^2U-\mathrm{i}\beta_1\frac{\partial}{\partial\tau}\left(|U|^2U\right)+\mathrm{i}\beta_2U\frac{\partial}{\partial\tau}\left(|U|^2\right)=0。\tag{60}$$

式(60)的系数($K_2$、$W$、$K_3$、$\beta_1$ 和 $\beta_2$)一般都为复数,通常很难获得其解析孤子解。采用简化式(52)时所选取的参数计算可得 $K_2=(-1.82\times10^{-27}+\mathrm{i}5.67\times10^{-29})\ \mu m^{-1}\cdot s^2$、$W=(-7.22\times10^{-28}+\mathrm{i}8.99\times10^{-30})\ \mu m^{-1}\cdot s^2$、$K_3=(1.04\times10^{-40}-\mathrm{i}4.10\times10^{-42})\ \mu m^{-1}\cdot s^3$、$\beta_1=(3.30\times10^{-41}-\mathrm{i}5.66\times10^{-43})\ \mu m^{-1}\cdot s^3$、$\beta_2=(2.37\times10^{-41}-\mathrm{i}3.04\times10^{-43})\ \mu m^{-1}\cdot s^3$。这些系数的实部都远大于虚部,即 $|K_{2r}|\gg|K_{2i}|$、$|W_r|\gg|W_i|$、$|K_{3r}|\gg|K_{3i}|$、$|\beta_{1r}|\gg|\beta_{1i}|$ 和 $|\beta_{2r}|\gg|\beta_{2i}|$,故式(60)中的系数 $K_2$、$W$、$K_3$、$\beta_1$ 和 $\beta_2$ 可分别用它们的实部 $K_{2r}$、$W_r$、$K_{3r}$、$\beta_{1r}$ 和 $\beta_{2r}$ 表示。随后,引入无量纲参量 $d_j=2L_D/L_j\ (j=0,1,2,3,4)$、$s=-z/(2L_D)$、$\sigma=\tau/\tau_0$、$u=U/U_0$,高阶非线性薛定谔方程[式(60)]简化为以下无量纲形式:

$$\mathrm{i}\frac{\partial u}{\partial s}+\frac{\partial^2u}{\partial\sigma^2}+2u|u|^2=\mathrm{i}\left[d_0u+d_1\frac{\partial\left(|u|^2u\right)}{\partial\sigma}+d_2u\frac{\partial\left(|u|^2\right)}{\partial\sigma}+d_3\frac{\partial^3u}{\partial\sigma^3}\right]+d_4\frac{\partial u}{\partial\sigma}。\tag{61}$$

此外,$L_0=2/\alpha$ 为特征吸收长度,$L_1=\tau_0^3W_r/(\beta_{1r}K_{2r})$ 为非线性色散长度,$L_2=\tau_0^3W_r/(\beta_{2r}K_{2r})$ 为非线性折射率延迟长度,$L_3=6\tau_0^3/K_{3r}$ 为三阶色散长度,$L_4=\tau_0/K_{1i}$ 为导数吸收长度。类似地,在推导式(61)的过程中,已经假定 $L_D=L_{NL}$,表示系统的色散效应和非线性效应平衡。因此,探测光的特征半拉比频率为 $U_0=(1/\tau_0)\sqrt{K_{2r}/W_r}$。需要注意的是,当 $\tau_0=1\times10^{-13}$ s 时,$L_0=25.25\ \mu m$ 和 $L_4=98.03\ \mu m$ 大于

$L_D=5.49\ \mu m$，因此式(61)右侧的 $d_0$ 和 $d_4$ 可被忽略，式(61)可化为

$$i\frac{\partial u}{\partial s}+\frac{\partial^2 u}{\partial \sigma^2}+2u|u|^2=i\left[d_1\frac{\partial\left(|u|^2u\right)}{\partial\sigma}+d_2u\frac{\partial|u|^2}{\partial\sigma}+d_3\frac{\partial^3u}{\partial\sigma^3}\right]。\tag{62}$$

通过求解式(62)，再返回原始变量，可得到计及高阶效应时的基本孤子解[35-37,40]，即

$$\Omega_{p1}(z,t)=U_0\sqrt{\frac{3(\beta+3q^2-2q)}{d_3^2(3c_1+c_2)}}\,\mathrm{sech}\left[\frac{\sqrt{\beta+3q^2-2q}}{d_3}\left(\frac{t-z/V_{gr}}{\tau_0}+\frac{\beta z}{2d_3L_D}\right)\right]\cdot$$
$$\exp\left\{i\left[q^3-q^2+(\beta+3q^2-2q)(1-3q)\right]\frac{z}{2d_3^2L_D}-i\frac{q}{d_3}\cdot\frac{t-z/V_{gr}}{\tau_0}+iK_{0r}z\right\},\tag{63}$$

式中：$q=(3c_1+2c_2-3)/[6(c_1+c_2)]$，$c_1=d_1/(2d_3)$，$c_2=d_2/(2d_3)$；$\beta$ 为任一实数。式(63)有孤子解的条件为 $\beta+3q^2-2q>0$ 且 $q\neq1/3$。

图 4 所示为孤子解[式(63)]所描述的探测光光强的幅度 $\left|\Omega_{p1}/U_0\right|^2$ 随时间 $t$ 演化的情况。图 4 中实线、短划线、短点线、点划线分别表示初始状态以及演化 0.5、1.0 和 1.5 个单位长度时的结果。可以看出，随着时间的推移，光孤子向右传播：当光孤子向右传播至 $z/(2L_D)=0.5$ 处(图 4 中短划线)时，孤子的振幅稍微降低；当光孤子向右传播至 $z/(2L_D)=1.0$ 处(图 4 中短点线)时，其孤子振幅与 $z/(2L_D)=0.5$ 处相比保持不变；当光孤子继续向右传播至 $z/(2L_D)=1.5$ 处(图 4 中点划线)时，其孤子振幅与 $z/(2L_D)=1.0$ 处相比仍然保持不变。从这一系列演化过程可归纳出，计及高阶效应时所形成的光孤子的波形保持不变且可比体系考虑低阶效应时所形成的光孤子(图 3)稳定地传播更长的距离，其主要原因是入射的探测光脉冲宽度较短，高阶非线性薛定谔方程中的高阶效应，包括三阶色散

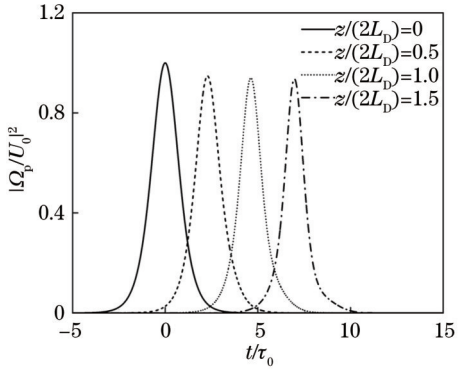


图 4　计及高阶效应时的光孤子稳定性分析

Fig. 4　Stability analysis of optical soliton with high-order effects

和非瞬时克尔效应，将会分别引起脉冲在时间与光谱上产生不对称展宽和脉冲的红移增加，从而不能被当作微扰处理[35,37,39]。图 4 中所使用的参数与图 3 相同。

## 5　光的存储与读取

由于计及高阶效应时所形成的光孤子可以在 N 型四能级非对称双量子阱体系内稳定地传播，因此探究该体系对探测光的存储和读取。以孤子解[式(63)]为初始条件，使用龙格-库塔法对 M-B 方程[式(2)～(12)]进行数值模拟。图 5 所示为不同探测光的 $|\Omega_{p1}\tau_0|$ 随时间 $t$ 和传播距离 $z$ 的变化函数。为了实现对光的存储，需要操控两束控制光，它们的开、关由以下的双曲正切函数表示，即

$$\Omega_b(0,t)=\Omega_{b0}\left[1-\frac{1}{2}\tanh\left(\frac{t-T_{off}}{T_s}\right)+\frac{1}{2}\tanh\left(\frac{t-T_{on}}{T_s}\right)\right],\tag{64}$$

$$\Omega_c(0,t)=\Omega_{c0}\left[1-\frac{1}{2}\tanh\left(\frac{t-T_{off}}{T_s}\right)+\frac{1}{2}\tanh\left(\frac{t-T_{on}}{T_s}\right)\right],\tag{65}$$

式中：$\Omega_{b0}$ 和 $\Omega_{c0}$ 均为常数，表示两束控制光的强度；$T_{off}$ 和 $T_{on}$ 分别为控制光的关闭和开启时间；$T_s$ 为操控控制光所需的时间。图 5 中所用的参数为 $\Omega_{b0}\tau_0=8$、$\Omega_{c0}\tau_0=24$、$T_s/\tau_0=1.1$、$T_{off}/\tau_0=6$、$T_{on}/\tau_0=18$，其他参数与图 3 相同。

图 5(a)展示了弱探测光的存储与读取，即当探测光为 $\Omega_{p1}(0,t)\tau_0=1.0\exp(-i3.2t/\tau_0)\,\mathrm{sech}(1.03t/\tau_0)$ 时，此时探测光强比较弱。可以看出，此时探测光的存取可通过控制光的关闭和开启来加以控制。随着时间 $t$ 和空间 $z$ 的演化，探测光在存储前和读取后的峰值逐渐降低，波形逐渐变宽。此时，系统的色散效应大于非线性效应，这在量子信息存储的实际应用中将导致信息失真。

将体系的探测光强增加到 $\Omega_{p1}(0,t)\tau_0=3.95\exp(-i3.2t/\tau_0)\,\mathrm{sech}(1.03t/\tau_0)$，此时系统的非线性效应与色散效应平衡，体系能形成光孤子。图 5(b)展示了计及高阶效应时形成的光孤子的存储与读取。

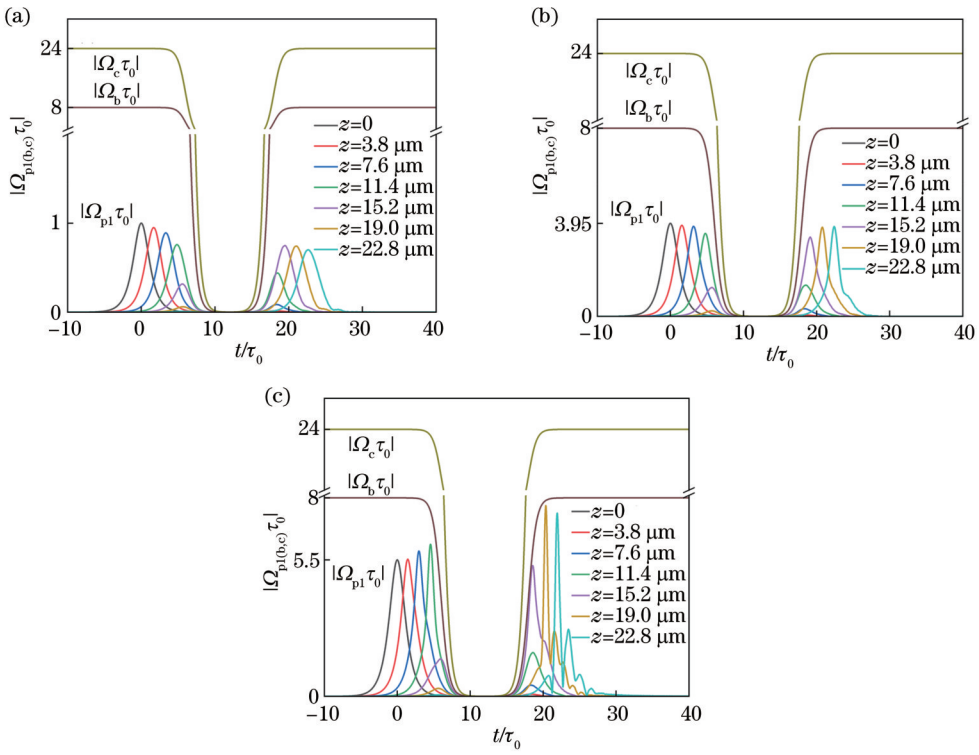


图 5　探测光的存储和读取。(a)弱光的存储与读取;(b)光孤子的存储和读取;(c)强光的存储与读取

Fig. 5　Storage and retrieval of control field. (a) Storage and retrieval of a weak pulse; (b) storage and retrieval of a soliton pulse; (c) storage and retrieval of a strong pulse

可以看出,读取后的波形与存储前几乎相同。这说明光孤子的存取同样可以通过控制光的关闭和开启来实现,即:当控制光关闭时,光孤子被存储在量子阱EIT介质中;在控制光开启后,对存储在介质中的光孤子进行读取。与此同时,从图5(b)所示曲线的形状也可得出,光孤子的存储与读取的保真度比光的存储与读取高。

继续增加体系的探测光强到 $\Omega_{p1}(0,t)\tau_0=5.5\exp(-\mathrm{i}3.2t/\tau_0)\mathrm{sech}(1.03t/\tau_0)$,此时系统的非线性效应强于色散效应。图5(c)展示了强探测光的存储与读取。可看出,强探测光的存取同样可通过控制光的关闭和开启控制,并且光脉冲读取后的峰值大于存储前的峰值,且波形聚拢。在这种情况下,探测光所携带的信息存在较严重的失真,这在实际运用中也极不理想。

从图5(a)~(c)能够看出,探测光的存储和读取可通过关闭和开启控制光来控制,其中弱探测光脉冲和强探测光脉冲在存储前和读取后的波形出现明显变形,导致光脉冲所携带的信息失真,只有光孤子脉冲在存储前和读取后的波形几乎没有改变,这说明光孤子存取的保真度要高于一般的光脉冲存取的保真度,是光信息存储的理想载体。因此,光孤子的存取具有更广泛的应用。更为重要的是,N型四能级非对称双量子阱体系中考虑低阶效应时形成的光孤子由于振幅衰减较快而不能被存储和读取,只有计及高阶效应时体系所形成的光孤子才能被体系存储和读取。

既然开启和关闭控制光可控制光孤子的存取,随后探究控制光强对体系光孤子存取幅度的影响。由于光孤子只能在EIT窗口下形成,而此体系只有开启第二控制光时才能形成EIT窗口,图6展示了仅开启第二控制光[图6(a)]及两束控制光都开启[图6(b)]时,光孤子存取的幅度随控制光强的变化情况。图6中所使用参数与图3相同。从图6(a)可看出,当第一控制光 $\Omega_b=0$ 时,光孤子的存取幅度随第二控制光强的增大而增加,并且当控制光强比较大时,光孤子的存取幅度最终会趋近于一个恒值。从图6(b)可以看到:当 $\Omega_b=5\times10^{13}\ \mathrm{s}^{-1}$ 时[图6(b)中实线],孤子幅度随第二控制光强的增大呈线性增长;从 $\Omega_b=10\times10^{13}\ \mathrm{s}^{-1}$[图6(b)中短划线]和 $\Omega_b=15\times10^{13}\ \mathrm{s}^{-1}$[图6(b)中短点线]的曲线中也可观察到类似的现象。同时,从与纵轴平行的虚线可看出:当第二控制光强保持不变时,第一控制光强为 $\Omega_b=15\times10^{13}\ \mathrm{s}^{-1}$ 的光孤子存取幅度比第一控制光强为 $\Omega_b=5\times10^{13}\ \mathrm{s}^{-1}$ 的光孤子存取幅度低;当第一控制光强增加到 $\Omega_b=15\times10^{13}\ \mathrm{s}^{-1}$ 时,此时光孤子存取幅度比第一控制光强为 $\Omega_b=10\times10^{13}\ \mathrm{s}^{-1}$ 的光孤子存取幅度低。这说明光孤子的存取幅度随着第一控制光强的增大而降低。

综上可知:当保持第一控制光的光强不变时,所存取光孤子的幅度随着第二控制光光强的增大而增加;

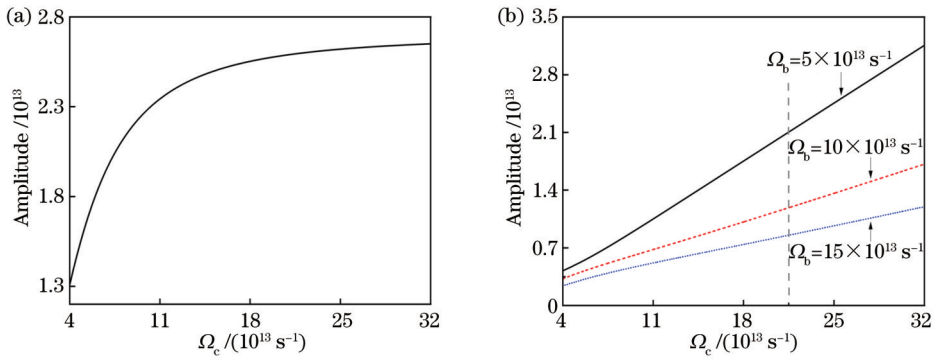


图 6　光孤子的存取幅度随第二控制光($\Omega_c$)和双控制光的变化情况。(a)第二控制光;(b)双控制光

Fig. 6　Amplitude of storage and retrieval of optical soliton as a function of the second ($\Omega_c$) and both control fields. (a) The second control field; (b) both control fields

当保持第二控制光的光强不变时,所存取光孤子的幅度随着第一控制光光强的增大而降低。由此可见,在N型四能级非对称双量子阱体系所存取的光孤子幅度可通过两束控制光的光强进行调节。

## 6　结　　论

首先,基于现有的实验条件构建了由一个$Al_{0.2}Ga_{0.8}As$薄势垒分隔的GaAs宽阱和窄阱组成的"三明治"型双量子阱模型。让弱探测光$\Omega_p$耦合到双量子阱的能级$|1\rangle$与$|3\rangle$之间,使第一控制光$\Omega_b$耦合到双量子阱的能级$|2\rangle$与$|4\rangle$之间,而第二控制光$\Omega_c$耦合到双量子阱的能级$|2\rangle$和$|3\rangle$之间,从而形成N型四能级非对称双量子阱EIT介质模型。然后,利用半经典理论结合多重尺度法获得体系的线性色散关系及非线性薛定谔方程,进而将非线性薛定谔方程的孤子解作为初始条件,利用龙格-库塔法研究了体系对探测光的存储和读取性质。结果发现,在线性情况下,关闭第二控制光时,无论第一控制光如何变化,体系的线性吸收特征曲线总是呈现洛伦兹吸收峰。只有开启第二控制光后,体系才会出现EIT窗口;若只开启第二控制光(即关闭第一控制光),体系仅仅为单一的EIT透明窗口,且单EIT窗口的宽度会随着第二控制光光强的增加而变宽。当两束控制光均开启后,体系会出现双EIT窗口,且任意一个控制光光强的增大均会使双EIT窗口的宽度变宽。有趣的是,当两束控制光均开启后,无论两束控制光的光强是否相等,双EIT窗口都呈对称分布。

在非线性情况下,考虑低阶效应时体系所形成的光孤子由于振幅衰减较快,不能长距离稳定地传播,因此不能被体系存储和读取,而光孤子的不稳定性正是由系统的高阶色散引起的。在计及高阶效应后,体系所形成的光孤子才会在体系中稳定地传播,且光孤子可通过关闭和开启控制光进行存储和读取。数值模拟结果表明,光孤子存取的保真度要高于一般的光脉冲存取的保真度。更为有趣的是:所存取的光孤子的幅度可通过控制光的光强进行调节,即当保持第一控制光的光强不变时,孤子幅度随第二控制光光强的增大而增加;保持第二控制光的光强不变时,孤子幅度随第一控制光强的增大而降低。这些结果为提高半导体量子阱器件中光量子信息存储和读取的保真度提供了一定的理论依据。

## 附录A

式(15)~(24)中$M^{(l)}$、$Y^{(l)}$、$Z^{(l)}$、$B^{(l)}$、$N^{(l)}$、$P^{(l)}$、$Q^{(l)}$、$H^{(l)}$、$J^{(l)}$、$G^{(l)}(l=1,2,3,4)$的表达式如下:

$$M^{(1)}=Y^{(1)}=Z^{(1)}=B^{(1)}=N^{(1)}=P^{(1)}=Q^{(1)}=H^{(1)}=J^{(1)}=G^{(1)}=0;$$

$$M^{(2)}=-\mathrm{i}\left(\frac{\partial}{\partial z_1}+\frac{1}{c}\cdot\frac{\partial}{\partial t_1}\right)\Omega_p^{(1)},\ Y^{(2)}=\Omega_p^{(1)}\rho_{31}^{*(1)}-\Omega_p^{*(1)}\rho_{31}^{(1)}-\mathrm{i}\frac{\partial}{\partial t_1}\rho_{11}^{(1)},\ Z^{(2)}=-\mathrm{i}\frac{\partial}{\partial t_1}\rho_{22}^{(1)},\ B^{(2)}=-\mathrm{i}\frac{\partial}{\partial t_1}\rho_{44}^{(1)},\ N^{(2)}=$$

$$\Omega_p^{(1)}\rho_{32}^{*(1)}-\mathrm{i}\frac{\partial}{\partial t_1}\rho_{21}^{(1)},\ P^{(2)}=\mathrm{i}\frac{\partial}{\partial t_1}\rho_{31}^{(1)}-\Omega_p^{(1)}\left[2\rho_{11}^{(1)}+\rho_{22}^{(1)}+\rho_{44}^{(1)}\right],\ Q^{(2)}=-\mathrm{i}\frac{\partial}{\partial t_1}\rho_{32}^{(1)}-\Omega_p^{(1)}\rho_{21}^{*(1)},\ H^{(2)}=\Omega_p^{(1)}\rho_{43}^{(1)}-i\frac{\partial}{\partial t_1}\rho_{41}^{(1)},$$

$$J^{(2)}=-\mathrm{i}\frac{\partial}{\partial t_1}\rho_{42}^{(1)},G^{(2)}=\Omega_p^{*(1)}\rho_{41}^{(1)}-\mathrm{i}\frac{\partial}{\partial t_1}\rho_{43}^{(1)};$$

$$M^{(3)}=-\mathrm{i}\left(\frac{\partial}{\partial z_1}+\frac{1}{c}\cdot\frac{\partial}{\partial t_1}\right)\Omega_p^{(2)}-\mathrm{i}\frac{\partial}{\partial z_2}\Omega_p^{(1)},\quad Y^{(3)}=\Omega_p^{(1)}\rho_{31}^{*(2)}+\Omega_p^{(2)}\rho_{31}^{*(1)}-\Omega_p^{*(1)}\rho_{31}^{(2)}-\Omega_p^{*(2)}\rho_{31}^{(1)}-\mathrm{i}\frac{\partial}{\partial t_1}\rho_{11}^{(2)},\quad Z^{(3)}=$$

$$-\mathrm{i}\frac{\partial}{\partial t_1}\rho_{22}^{(2)},\quad B^{(3)}=-\mathrm{i}\frac{\partial}{\partial t_1}\rho_{44}^{(2)},\quad N^{(3)}=\Omega_p^{(1)}\rho_{32}^{*(2)}+\Omega_p^{(2)}\rho_{32}^{*(1)}-\mathrm{i}\frac{\partial}{\partial t_1}\rho_{21}^{(2)},\quad P^{(3)}=\mathrm{i}\frac{\partial}{\partial t_1}\rho_{31}^{(2)}-\Omega_p^{(1)}\left[2\rho_{11}^{(2)}+\rho_{22}^{(2)}+\rho_{44}^{(2)}\right]-$$

$\Omega_{\mathrm{p}}^{(2)}\left[2\rho_{11}^{(1)}+\rho_{22}^{(1)}+\rho_{44}^{(1)}\right], Q^{(3)}=-\mathrm{i}\dfrac{\partial}{\partial t_1}\rho_{32}^{(2)}-\Omega_{\mathrm{p}}^{(1)}\rho_{21}^{*(2)}-\Omega_{\mathrm{p}}^{(2)}\rho_{21}^{*(1)}, H^{(3)}=\Omega_{\mathrm{p}}^{(1)}\rho_{43}^{(2)}+\Omega_{\mathrm{p}}^{(2)}\rho_{43}^{(1)}-i\dfrac{\partial}{\partial t_1}\rho_{41}^{(2)}, J^{(3)}=-\mathrm{i}\dfrac{\partial}{\partial t_1}\rho_{42}^{(2)},$

$G^{(3)}=\Omega_{\mathrm{p}}^{*(1)}\rho_{41}^{(2)}+\Omega_{\mathrm{p}}^{*(2)}\rho_{41}^{(1)}-\mathrm{i}\dfrac{\partial}{\partial t_1}\rho_{43}^{(2)};$

$M^{(4)}=-\mathrm{i}\left(\dfrac{\partial}{\partial z_1}+\dfrac{1}{c}\cdot\dfrac{\partial}{\partial t_1}\right)\Omega_{\mathrm{p}}^{(3)}-\mathrm{i}\dfrac{\partial}{\partial z_2}\Omega_{\mathrm{p}}^{(2)}-\mathrm{i}\dfrac{\partial}{\partial z_3}\Omega_{\mathrm{p}}^{(1)}, \quad Y^{(4)}=\Omega_{\mathrm{p}}^{(1)}\rho_{31}^{*(3)}+\Omega_{\mathrm{p}}^{(2)}\rho_{31}^{*(2)}+\Omega_{\mathrm{p}}^{(3)}\rho_{31}^{*(1)}-\Omega_{\mathrm{p}}^{*(1)}\rho_{31}^{(3)}-$

$\Omega_{\mathrm{p}}^{*(2)}\rho_{31}^{(2)}-\Omega_{\mathrm{p}}^{*(3)}\rho_{31}^{(1)}-\mathrm{i}\dfrac{\partial}{\partial t_1}\rho_{11}^{(3)}, Z^{(4)}=-\mathrm{i}\dfrac{\partial}{\partial t_1}\rho_{22}^{(3)}, B^{(4)}=-\mathrm{i}\dfrac{\partial}{\partial t_1}\rho_{44}^{(3)}, N^{(4)}=\Omega_{\mathrm{p}}^{(1)}\rho_{32}^{*(3)}+\Omega_{\mathrm{p}}^{(2)}\rho_{32}^{*(2)}+\Omega_{\mathrm{p}}^{(3)}\rho_{32}^{*(1)}-\mathrm{i}\dfrac{\partial}{\partial t_1}\rho_{21}^{(3)},$

$P^{(4)}=-\mathrm{i}\dfrac{\partial}{\partial t_1}\rho_{31}^{(3)}-\Omega_{\mathrm{p}}^{(1)}\left[2\rho_{11}^{(3)}+\rho_{22}^{(3)}+\rho_{44}^{(3)}\right]-\Omega_{\mathrm{p}}^{(2)}\left[2\rho_{11}^{(2)}+\rho_{22}^{(2)}+\rho_{44}^{(2)}\right]-\Omega_{\mathrm{p}}^{(3)}\left[2\rho_{11}^{(1)}+\rho_{22}^{(1)}+\rho_{44}^{(1)}\right], \quad Q^{(4)}=-\mathrm{i}\dfrac{\partial}{\partial t_1}\rho_{32}^{(3)}-$

$\Omega_{\mathrm{p}}^{(1)}\rho_{21}^{*(3)}-\Omega_{\mathrm{p}}^{(2)}\rho_{21}^{*(2)}-\Omega_{\mathrm{p}}^{(3)}\rho_{21}^{*(1)}, \quad H^{(4)}=\Omega_{\mathrm{p}}^{(1)}\rho_{43}^{(3)}+\Omega_{\mathrm{p}}^{(2)}\rho_{43}^{(2)}+\Omega_{\mathrm{p}}^{(3)}\rho_{43}^{(1)}-i\dfrac{\partial}{\partial t_1}\rho_{41}^{(3)}, \quad J^{(4)}=-\mathrm{i}\dfrac{\partial}{\partial t_1}\rho_{42}^{(3)}, \quad G^{(4)}=\Omega_{\mathrm{p}}^{*(1)}\rho_{41}^{(3)}+$

$\Omega_{\mathrm{p}}^{*(2)}\rho_{41}^{(2)}+\Omega_{\mathrm{p}}^{*(3)}\rho_{41}^{(1)}-\mathrm{i}\dfrac{\partial}{\partial t_1}\rho_{43}^{(3)}。$

## 附录 B

M-B方程组的多重尺度展开至二阶时，系数$A_{21}^{(2)}$、$A_{41}^{(2)}$、$A_{11}^{(2)}$、$A_{22}^{(2)}$、$A_{44}^{(2)}$、$A_{32}^{(2)}$、$A_{42}^{(2)}$、$A_{43}^{(2)}$的表达式如下：

$$A_{21}^{(2)}=\frac{\Omega_{\mathrm{c}}^{*}(\omega+d_{41})}{k_{13}D_{\mathrm{p}}}\left(K_1-\frac{1}{c}\right)-\frac{|\Omega_{\mathrm{b}}|^2\Omega_{\mathrm{c}}^{*}+\Omega_{\mathrm{c}}^{*}(\omega+d_{41})^2}{D_{\mathrm{p}}D},$$

$$A_{41}^{(2)}=\frac{\Omega_{\mathrm{b}}\Omega_{\mathrm{c}}^{*}(\omega+d_{41})+\Omega_{\mathrm{b}}\Omega_{\mathrm{c}}^{*}(\omega+d_{21})}{D_{\mathrm{p}}D}-\frac{\Omega_{\mathrm{b}}\Omega_{\mathrm{c}}^{*}}{k_{13}D_{\mathrm{p}}}\left(K_1-\frac{1}{c}\right),$$

$$A_{11}^{(2)}=\frac{\dfrac{|\Omega_{\mathrm{b}}|^2|\Omega_{\mathrm{c}}|^2}{X_0D^{*}}-\dfrac{(\omega+d_{41})|\Omega_{\mathrm{c}}|^2}{d_{32}^{*}D}-\dfrac{\Omega_{\mathrm{b}}^{*}\Omega_{\mathrm{c}}}{X_1}T_0-\dfrac{d_{32}^{*}\Omega_{\mathrm{c}}T_{11}}{X_1}T_0-\dfrac{T_{10}}{X_3}T_5+\dfrac{T_{12}}{X_4}T_6+\dfrac{X_4T_{13}}{\mathrm{i}\Gamma_{13}(X_4-T_8)}T_9}{\mathrm{i}\Gamma_{23}-\dfrac{|\Omega_{\mathrm{c}}|^2}{d_{32}^{*}}-\dfrac{|\Omega_{\mathrm{b}}|^2|\Omega_{\mathrm{c}}|^2}{d_{32}^{*}X_1}-\dfrac{\Omega_{\mathrm{b}}|\Omega_{\mathrm{c}}|^2T_{11}}{X_1}-\dfrac{\Omega_{\mathrm{c}}T_{10}}{X_3}+\dfrac{T_7T_{12}}{X_4}-\dfrac{(T_7-X_4)T_{13}}{X_4-T_8}},$$

$$A_{22}^{(2)}=\frac{X_4T_9+\mathrm{i}\Gamma_{13}(T_7-X_4)A_{11}^{(2)}}{\mathrm{i}\Gamma_{13}(X_4-T_8)},$$

$$A_{44}^{(2)}=\frac{T_6-T_7A_{11}^{(2)}-T_8A_{22}^{(2)}}{X_4},$$

$$A_{32}^{(2)}=\frac{T_5-\Omega_{\mathrm{c}}A_{11}^{(2)}-T_3A_{22}^{(2)}+T_4A_{44}^{(2)}}{X_3},$$

$$A_{42}^{(2)}=X_1\left[\frac{d_{32}^{*}\Omega_{\mathrm{c}}}{X_1}T_0-\frac{\Omega_{\mathrm{b}}|\Omega_{\mathrm{c}}|^2}{X_1}A_{11}^{(2)}-T_1A_{22}^{(2)}+T_2A_{44}^{(2)}\right],$$

$$A_{43}^{(2)}=\frac{d_{32}^{*}}{X_1}\left[T_0+\Omega_{\mathrm{c}}^{*}A_{42}^{(2)}-\frac{\Omega_{\mathrm{b}}\Omega_{\mathrm{c}}^{*}}{d_{32}^{*}}A_{11}^{(2)}-\frac{2\Omega_{\mathrm{b}}\Omega_{\mathrm{c}}^{*}}{d_{32}^{*}}A_{22}^{(2)}-\frac{\Omega_{\mathrm{b}}\Omega_{\mathrm{c}}^{*}}{d_{32}^{*}}A_{44}^{(2)}\right]。$$

其中，$X_0=d_{42}^{*}d_{43}^{*}-|\Omega_{\mathrm{c}}|^2$，$X_1=d_{43}d_{32}^{*}-|\Omega_{\mathrm{b}}|^2$，$X_2=\dfrac{X_1}{d_{42}X_1-d_{32}^{*}|\Omega_{\mathrm{c}}|^2}$，$X_3=d_{32}-\dfrac{|\Omega_{\mathrm{b}}|^2}{d_{43}^{*}}-\dfrac{|\Omega_{\mathrm{b}}|^2|\Omega_{\mathrm{c}}|^2}{d_{43}^{*}X_0}$，$X_4=\mathrm{i}\Gamma_{24}-$

$\dfrac{d_{43}^{*}|\Omega_{\mathrm{b}}|^2}{X_0}-\Omega_{\mathrm{b}}^{*}X_2T_2-\dfrac{|\Omega_{\mathrm{b}}|^2\Omega_{\mathrm{c}}^{*}T_4}{X_0X_3}$，$T_0=\dfrac{\Omega_{\mathrm{b}}\Omega_{\mathrm{c}}^{*}}{D}+\dfrac{(\omega+d_{41})\Omega_{\mathrm{b}}\Omega_{\mathrm{c}}^{*}}{d_{32}^{*}D}$，$T_1=\Omega_{\mathrm{b}}+\dfrac{2\Omega_{\mathrm{b}}|\Omega_{\mathrm{c}}|^2}{X_1}$，$T_2=\Omega_{\mathrm{b}}-\dfrac{\Omega_{\mathrm{b}}|\Omega_{\mathrm{c}}|^2}{X_1}$，$T_3=$

$2\Omega_{\mathrm{c}}+\dfrac{|\Omega_{\mathrm{b}}|^2\Omega_{\mathrm{c}}}{X_0}$，$T_4=\dfrac{|\Omega_{\mathrm{b}}|^2\Omega_{\mathrm{c}}}{X_0}-\Omega_{\mathrm{c}}$，$T_5=\dfrac{(\omega+d_{41}^{*})\Omega_{\mathrm{c}}}{D^{*}}-\left(\dfrac{\Omega_{\mathrm{b}}}{d_{43}^{*}}+\dfrac{\Omega_{\mathrm{b}}|\Omega_{\mathrm{c}}|^2}{d_{43}^{*}X_0}\right)\dfrac{\Omega_{\mathrm{b}}^{*}\Omega_{\mathrm{c}}}{D^{*}}$，$T_6=\dfrac{d_{32}^{*}\Omega_{\mathrm{b}}^{*}\Omega_{\mathrm{c}}X_2}{X_1}T_0-$

$\dfrac{|\Omega_{\mathrm{b}}|^2|\Omega_{\mathrm{c}}|^2}{X_0D^{*}}+\dfrac{|\Omega_{\mathrm{b}}|^2\Omega_{\mathrm{c}}^{*}}{X_0X_3}T_5$，$T_7=\dfrac{|\Omega_{\mathrm{b}}|^2|\Omega_{\mathrm{c}}|^2X_2}{X_1}+\dfrac{|\Omega_{\mathrm{b}}|^2|\Omega_{\mathrm{c}}|^2}{X_0X_3}$，$T_8=\dfrac{d_{43}^{*}|\Omega_{\mathrm{b}}|^2}{X_0}+\Omega_{\mathrm{b}}^{*}X_2T_1+\dfrac{|\Omega_{\mathrm{b}}|^2\Omega_{\mathrm{c}}^{*}T_3}{X_0X_3}$，$T_9=\left(\dfrac{D_{\mathrm{p}}}{D}-\right.$

$\left.\dfrac{D_{\mathrm{p}}^{*}}{D^{*}}\right)-\dfrac{\mathrm{i}\Gamma_{13}}{X_4}T_6$，$T_{10}=\Omega_{\mathrm{c}}^{*}+\dfrac{|\Omega_{\mathrm{b}}|^2\Omega_{\mathrm{c}}^{*}}{X_0}$，$T_{11}=\Omega_{\mathrm{b}}^{*}X_2+\dfrac{\Omega_{\mathrm{b}}^{*}|\Omega_{\mathrm{c}}|^2X_2}{X_1}$，$T_{12}=\mathrm{i}\Gamma_{24}-\mathrm{i}\Gamma_{23}-\dfrac{d_{43}^{*}|\Omega_{\mathrm{b}}|^2}{X_0}+\dfrac{|\Omega_{\mathrm{c}}|^2}{d_{32}^{*}}+$

$\frac{|\Omega_b|^2|\Omega_c|^2}{d_{32}^* X_1}-T_{11}T_2-\frac{T_4T_{10}}{X_3}$，$T_{13}=\frac{d_{43}^*|\Omega_b|^2}{X_0}-\mathrm{i}\Gamma_{23}+\frac{2|\Omega_c|^2}{d_{32}^*}+\frac{2|\Omega_b|^2|\Omega_c|^2}{d_{32}^* X_1}+T_{11}T_1+\frac{T_3T_{10}}{X_3}-\frac{T_8T_{12}}{X_4}$。

## 附录C

M-B方程组的多重尺度展开至三阶时，系数$A_{31'}^{(3)}$、$A_{31''}^{(3)}$、$A_{21'}^{(3)}$、$A_{21''}^{(3)}$、$A_{41'}^{(3)}$、$A_{41''}^{(3)}$、$A_{11'}^{(3)}$、$A_{11''}^{(3)}$、$A_{22'}^{(3)}$、$A_{22''}^{(3)}$、$A_{44'}^{(3)}$、$A_{44''}^{(3)}$、$A_{32'}^{(3)}$、$A_{32''}^{(3)}$、$A_{42'}^{(3)}$、$A_{42''}^{(3)}$、$A_{43'}^{(3)}$、$A_{43''}^{(3)}$的表达式如下：

$$A_{31'}^{(3)}=\frac{D_p(K_1-1/c)+k_{13}(\omega+d_{41})A_{21}^{(2)}-k_{13}\Omega_b^*\Omega_c A_{41}^{(2)}}{k_{13}D},A_{31''}^{(3)}=\frac{J_w}{D};$$

$$A_{21'}^{(3)}=\frac{(\omega+d_{41})\Omega_c^* A_{31'}^{(3)}+\Omega_b^* A_{41}^{(2)}-(\omega+d_{41})A_{21}^{(2)}}{D_p},A_{21''}^{(3)}=\frac{\Omega_b^* A_{43}^{(2)}-(\omega+d_{41})\Omega_c^* A_{31''}^{(3)}-(\omega+d_{41})A_{32}^{*(2)}}{D_p};$$

$$A_{41'}^{(3)}=\frac{\Omega_b A_{21}^{(2)}-(\omega+d_{21})A_{41}^{(2)}-\Omega_b\Omega_c^* A_{31'}^{(3)}}{D_p},A_{41''}^{(3)}=\frac{\Omega_b A_{32}^{*(2)}-(\omega+d_{21})A_{43}^{(2)}+\Omega_b\Omega_c^* A_{31''}^{(3)}}{D_p};$$

$$A_{11'}^{(3)}=\frac{T_{24'}+T_{25'}}{X_8},A_{11''}^{(3)}=\frac{T_{24''}+T_{25''}}{X_8};$$

$$A_{22'}^{(3)}=\frac{X_7T_{20'}+\mathrm{i}\Gamma_{13}(T_{18}-X_7)A_{11'}^{(3)}}{\mathrm{i}\Gamma_{13}(X_7-T_{19})},A_{22''}^{(3)}=\frac{X_7T_{20''}+\mathrm{i}\Gamma_{13}(T_{18}-X_7)A_{11''}^{(3)}}{\mathrm{i}\Gamma_{13}(X_7-T_{19})};$$

$$A_{44'}^{(3)}=\frac{T_{17'}-T_{18}A_{11'}^{(3)}-T_{19}A_{22'}^{(3)}}{X_7},A_{44''}^{(3)}=\frac{T_{17''}-T_{18}A_{11''}^{(3)}-T_{19}A_{22''}^{(3)}}{X_7};$$

$$A_{32'}^{(3)}=\frac{d_{43}^* X_0}{X_6}\left[T_{16'}-\Omega_c A_{11'}^{(3)}-T_3A_{22'}^{(3)}+T_4A_{44'}^{(3)}\right],A_{32''}^{(3)}=\frac{d_{43}^* X_0}{X_6}\left[T_{16''}-\Omega_c A_{11''}^{(3)}-T_3A_{22''}^{(3)}+T_4A_{44''}^{(3)}\right];$$

$$A_{42'}^{(3)}=\frac{X_1}{X_5}\left[T_{14'}-\frac{\Omega_b|\Omega_c|^2}{X_1}A_{11'}^{(3)}-T_1A_{22'}^{(3)}+T_2A_{44'}^{(3)}\right],A_{42''}^{(3)}=\frac{X_1}{X_5}\left[T_{14''}-\frac{\Omega_b|\Omega_c|^2}{X_1}A_{11''}^{(3)}-T_1A_{22''}^{(3)}+T_2A_{44''}^{(3)}\right];$$

$$A_{43'}^{(3)}=\frac{d_{32}^*}{X_1}\left\{A_{41}^{(2)}-A_{43}^{(2)}-\frac{\Omega_b}{d_{32}^*}\left[A_{21}^{(2)}-A_{32}^{*(2)}\right]+\Omega_c^* A_{42'}^{(3)}-\frac{\Omega_b\Omega_c^*}{d_{32}^*}A_{11'}^{(3)}-\frac{2\Omega_b\Omega_c^*}{d_{32}^*}A_{22'}^{(3)}-\frac{\Omega_b\Omega_c^*}{d_{32}^*}A_{44'}^{(3)}\right\},$$

$$A_{43''}^{(3)}=\frac{d_{32}^*}{X_1}\left[A_{43}^{(2)}-\frac{\Omega_b}{d_{32}^*}A_{32}^{*(2)}+\Omega_c^* A_{42''}^{(3)}-\frac{\Omega_b\Omega_c^*}{d_{32}^*}A_{11''}^{(3)}-\frac{2\Omega_b\Omega_c^*}{d_{32}^*}A_{22''}^{(3)}-\frac{\Omega_b\Omega_c^*}{d_{32}^*}A_{44''}^{(3)}\right]。$$

其中，$X_5=d_{42}X_1-d_{32}^*|\Omega_c|^2$，$X_6=d_{32}d_{43}^*X_0-|\Omega_b|^2X_0-|\Omega_b|^2|\Omega_c|^2$，$X_7=\mathrm{i}\Gamma_{24}-\frac{d_{43}^*|\Omega_b|^2}{X_0}-\frac{\Omega_b^*X_1T_2}{X_5}-\frac{d_{43}^*|\Omega_b|^2\Omega_c^*T_4}{X_6}$，$X_8=\mathrm{i}\Gamma_{23}-\frac{|\Omega_c|^2}{d_{32}^*}-\frac{|\Omega_b|^2|\Omega_c|^2}{d_{32}^*X_1}-\frac{\Omega_b|\Omega_c|^2T_{21}}{X_1}-\frac{d_{43}^*\Omega_cX_0T_{10}}{X_6}+\frac{T_{18}T_{22}}{X_7}-\frac{(T_{18}-X_7)T_{23}}{X_7-T_{19}}$，$T_{14'}=\frac{d_{32}^*\Omega_c}{X_1}\left[A_{41}^{(2)}-A_{43}^{(2)}\right]-A_{42}^{(2)}-\frac{\Omega_b\Omega_c}{X_1}\left[A_{21}^{(2)}-A_{32}^{*(2)}\right]$，$T_{14''}=\frac{d_{32}^*\Omega_c}{X_1}A_{43}^{(2)}+A_{42}^{(2)}-\frac{\Omega_b\Omega_c}{X_1}A_{32}^{*(2)}$，$T_{15}=\frac{\Omega_b}{d_{43}^*}+\frac{\Omega_b|\Omega_c|^2}{d_{43}^*X_0}$，$T_{16'}=\frac{\Omega_b\Omega_c}{X_0}A_{42}^{*(2)}-A_{32}^{(2)}-T_{15}A_{43}^{*(2)}$，$T_{16''}=A_{32}^{(2)}-A_{21}^{*(2)}-\frac{\Omega_b\Omega_c}{X_0}A_{42}^{*(2)}+T_{15}\left[A_{43}^{*(2)}-A_{41}^{*(2)}\right]$，$T_{17'}=\frac{X_1\Omega_b^*}{X_5}T_{14'}-A_{44}^{(2)}-\frac{\Omega_b\Omega_c^*}{X_0}A_{43}^{*(2)}+\frac{d_{43}^*\Omega_b}{X_0}A_{42}^{*(2)}+\frac{d_{43}^*|\Omega_b|^2\Omega_c^*}{X_6}T_{16'}$，$T_{17''}=\frac{X_1\Omega_b^*}{X_5}T_{14''}+A_{44}^{(2)}+\frac{\Omega_b\Omega_c^*}{X_0}\left[A_{43}^{*(2)}-A_{41}^{*(2)}\right]-\frac{d_{43}^*\Omega_b}{X_0}A_{42}^{*(2)}+\frac{d_{43}^*|\Omega_b|^2\Omega_c^*}{X_6}T_{16''}$，$T_{18}=\frac{|\Omega_b|^2|\Omega_c|^2}{X_5}+\frac{d_{43}^*|\Omega_b|^2|\Omega_c|^2}{X_6}$，$T_{19}=\frac{d_{43}^*|\Omega_b|^2}{X_0}+\frac{\Omega_b^*X_1T_1}{X_5}+\frac{d_{43}^*|\Omega_b|^2\Omega_c^*T_3}{X_6}$，$T_{20'}=-\frac{1}{k_{13}}\left(\frac{1}{V_g}-\frac{1}{c}\right)-A_{11}^{(2)}-\frac{\mathrm{i}\Gamma_{13}}{X_7}T_{17'}$，$T_{20''}=\frac{1}{k_{13}}\left(\frac{1}{V_g}-\frac{1}{c}\right)+A_{11}^{(2)}-\frac{\mathrm{i}\Gamma_{13}}{X_7}T_{17''}$，$T_{21}=\frac{\Omega_b^*}{X_5}\left(X_1+|\Omega_c|^2\right)$，$T_{22}=\mathrm{i}\Gamma_{24}-\mathrm{i}\Gamma_{23}-\frac{d_{43}^*|\Omega_b|^2}{X_0}+\frac{|\Omega_c|^2}{d_{32}^*}+\frac{|\Omega_b|^2|\Omega_c|^2}{d_{32}^*X_1}-T_2T_{21}-\frac{d_{43}^*X_0T_4T_{10}}{X_6}$，$T_{23}=\frac{d_{43}^*|\Omega_b|^2}{X_0}-\mathrm{i}\Gamma_{23}+\frac{2|\Omega_c|^2}{d_{32}^*}+\frac{2|\Omega_b|^2|\Omega_c|^2}{d_{32}^*X_1}+T_1T_{21}+\frac{d_{43}^*X_0T_3T_{10}}{X_6}-\frac{T_{19}T_{22}}{X_7}$，$T_{24'}=\left(\frac{\Omega_c}{d_{32}^*}+\frac{|\Omega_b|^2\Omega_c}{d_{32}^*X_1}\right)\left[A_{21}^{(2)}-A_{32}^{*(2)}\right]-A_{22}^{(2)}-\frac{\Omega_bd_{43}^*}{X_0}A_{42}^{*(2)}+\frac{\Omega_b\Omega_c^*}{X_0}A_{43}^{*(2)}-\frac{\Omega_b^*\Omega_c}{X_1}\left[A_{41}^{(2)}-A_{43}^{(2)}\right]$，$T_{24''}=\left(\frac{\Omega_c}{d_{32}^*}+\right.$

$$\left(\frac{|\Omega_b|^2\Omega_c}{d_{32}^* X_1}\right)A_{32}^{*(2)}+A_{22}^{(2)}+\frac{\Omega_b d_{43}^*}{X_0}A_{42}^{*(2)}-\frac{\Omega_b\Omega_c^*}{X_0}\left[A_{43}^{*(2)}-A_{41}^{*(2)}\right]-\frac{\Omega_b^*\Omega_c}{X_1}A_{43}^{(2)},\quad T_{25'}=\frac{T_{22}}{X_7}T_{17'}-T_{21}T_{14'}-\frac{d_{43}^* X_0 T_{10}}{X_6}T_{16'}+\frac{X_7 T_{23}}{\mathrm{i}\Gamma_{13}(X_7-T_{19})}T_{20'},T_{25''}=\frac{T_{22}}{X_7}T_{17''}-T_{21}T_{14''}-\frac{d_{43}^* X_0 T_{10}}{X_6}T_{16''}+\frac{X_7 T_{23}}{\mathrm{i}\Gamma_{13}(X_7-T_{19})}T_{20''}。$$

## 参 考 文 献


[1] Liu C, Dutton Z, Behroozi C H, et al. Observation of coherent optical information storage in an atomic medium using halted light pulses[J]. Nature, 2001, 409(6819): 490-493.

[2] Phillips D F, Fleischhauer A, Mair A, et al. Storage of light in atomic vapor[J]. Physical Review Letters, 2001, 86(5): 783-786.

[3] Winbow A G, Hammack A T, Butov L V, et al. Photon storage with nanosecond switching in coupled quantum well nanostructures[J]. Nano Letters, 2007, 7(5): 1349-1351.

[4] Haus H A, Wong W S. Solitons in optical communications[J]. Reviews of Modern Physics, 1996, 68(2): 423-444.

[5] Wu Y, Deng L. Ultraslow optical solitons in a cold four-state medium[J]. Physical Review Letters, 2004, 93(14): 143904.

[6] Huang G X, Jiang K J, Payne M G, et al. Formation and propagation of coupled ultraslow optical soliton pairs in a cold three-state double-Λ system[J]. Physical Review E, 2006, 73(5): 056606.

[7] 罗婷婷, 王登龙, 佘彦超, 等. 量子点中两耦合时间矢量光孤子的碰撞特性[J]. 光学学报, 2016, 36(2): 0227001.
Luo T T, Wang D L, She Y C, et al. Collision characteristics of two coupled temporal vector optical solitons in quantum dot [J]. Acta Optica Sinica, 2016, 36(2): 0227001.

[8] Dong Y Y, Wang D L, Wang Y, et al. Matching group velocity of bright and/or dark solitons via double-dark resonances[J]. Physics Letters A, 2018, 382(30): 2006-2012.

[9] 王苗, 杭超. 脉冲内四波混频与四分量超慢光孤子[J]. 光学学报, 2018, 38(10): 1019001.
Wang M, Hang C. Intrapulse four-wave mixing and four-component ultraslow optical solitons[J]. Acta Optica Sinica, 2018, 38(10): 1019001.

[10] 白娟, 杨荣草, 田晋平. 超材料中高阶效应影响下飞秒准亮孤子解及其特性[J]. 光学学报, 2020, 40(2): 0219001.
Bai J, Yang R C, Tian J P. Femtosecond quasi-bright soliton solution and its properties under influence of higher-order effects in metamaterials[J]. Acta Optica Sinica, 2020, 40(2): 0219001.

[11] Zhang X F, Yang Q, Zhang J F, et al. Controlling soliton interactions in Bose-Einstein condensates by synchronizing the Feshbach resonance and harmonic trap[J]. Physical Review A, 2008, 77(2): 023613.

[12] Hang C, Huang G X. Parity-time symmetry along with nonlocal optical solitons and their active controls in a Rydberg atomic gas [J]. Physical Review A, 2018, 98(4): 043840.

[13] Li Z D, Wang Y Y, He P B. Formation mechanism of asymmetric breather and rogue waves in pair-transition-coupled nonlinear Schrödinger equations[J]. Chinese Physics B, 2019, 28(1): 010504.

[14] Wang Y, Ding J W, Wang D L. Controllable double tunneling induced optical soliton storage in linear triple quantum dot molecules[J]. The European Physical Journal D, 2020, 74(9): 190-197.

[15] 田湘椿, 谭超华. 相干介质中基于矩形势垒调制全光开关的研究[J]. 光学学报, 2022, 42(21): 2126005.
Tian X C, Tan C H. Research on all-optical switch based on moment barrier modulation in coherent media[J]. Acta Optica Sinica, 2022, 42(21): 2126005.

[16] Zhou S J, Wang D L, Dong Y Y, et al. Controllable storage and retrieval of optical solitons in triple quantum dot molecules by inter-dot tunneling coupling effect[J]. Physics Letters A, 2022, 448(1): 128320.

[17] Bai Z Y, Hang C, Huang G X. Storage and retrieval of ultraslow optical solitons in coherent atomic system[J]. Chinese Optics Letters, 2013, 11(1): 012701.

[18] Chen Y, Bai Z Y, Huang G X. Ultraslow optical solitons and their storage and retrieval in an ultracold ladder-type atomic system[J]. Physical Review A, 2014, 89(2): 023835.

[19] Hang C, Huang G X. Weak-light ultraslow vector solitons via electromagnetically induced transparency[J]. Physical Review A, 2008, 77(3): 033830.

[20] Dong Y Y, Zheng X J, Wang D L, et al. Fluctuation-enhanced Kerr nonlinearity in an atom-assisted optomechanical system with atom-cavity interactions[J]. Optics Express, 2021, 29(4): 5367-5383.

[21] 关佳, 朱成杰. $Pr^{3+}$:$Y_2SiO_5$掺杂波导中的电磁诱导透明现象[J]. 光学学报, 2022, 42(21): 2126009.
Guan J, Zhu C J. Electromagnetic induced transparency in $Pr^{3+}$:$Y_2SiO_5$ doped waveguide[J]. Acta Optica Sinica, 2022, 42(21): 2126009.

[22] Chen Y, Chen Z M, Huang G X. Storage and retrieval of vector optical solitons via double electromagnetically induced transparency[J]. Physical Review A, 2015, 91(2): 023820.

[23] Shou C, Huang G X. Slow-light soliton beam splitters[J]. Physical Review A, 2019, 99(4): 043821.

[24] Ku P C, Sedgwick F, Chang-Hasnain C J, et al. Slow light in semiconductor quantum wells[J]. Optics Letters, 2004, 29(19): 2291-2293.

[25] Winbow A G, Butov L V, Gossard A C. Photon storage with subnanosecond readout rise time in coupled quantum wells[J]. Journal of Applied Physics, 2008, 104(6): 063515.

[26] Simon C, Afzelius M, Appel J, et al. Quantum memories: a review based on the European integrated project "qubit applications (QAP)"[J]. The European Physical Journal D, 2010, 58(1): 1-22.

[27] Phillips M, Wang H L. Electromagnetically induced transparency due to intervalence band coherence in a GaAs quantum well[J]. Optics Letters, 2003, 28(10): 831-833.

[28] Frogley M D, Dynes J F, Beck M, et al. Gain without inversion in semiconductor nanostructures[J]. Nature Materials, 2006, 5(3): 175-178.

[29] Li J H. Controllable optical bistability in a four-subband semiconductor quantum well system[J]. Physical Review B, 2007, 75(15): 155329.

[30] Wang Z P. Control of the optical multistability in a three-level ladder-type quantum well system[J]. Optics Communications, 2009, 282(24): 4745-4748.

[31] Sun H, Gong S Q, Niu Y P, et al. Enhancing Kerr nonlinearity in an asymmetric double quantum well via Fano interference[J]. Physical Review B, 2006, 74(15): 155314.

[32] 杜英杰, 杨战营, 谢小涛, 等. 电磁感应透明的高阶非线性效应对光孤子的影响[J]. 光学学报, 2015, 35(2): 0227002.
Du Y J, Yang Z Y, Xie X T, et al. Influence of higher nonlinearity to optical solitons in electromagnetically induced transparency medium[J]. Acta Optica Sinica, 2015, 35(2): 0227002.

[33] Yang W X, Hou J M, Lin Y Y, et al. Detuning management of optical solitons in coupled quantum wells[J]. Physical Review A, 2009, 79(3): 033825.

[34] 唐宏, 王登龙, 张蔚曦, 等. 纵波光学声子耦合对级联型电磁感应透明半导体量子阱中暗-亮光孤子类型的调控[J]. 物理学报, 2017, 66(3): 034202.
Tang H, Wang D L, Zhang W X, et al. Controlling of dark or bright soliton type in a cascade-type electromagnetically induced transparency semiconductor quantum well by the coupling longitudinal optical phonons[J]. Acta Physica Sinica, 2017, 66(3): 034202.

[35] Zhu C J, Huang G X. Slow-light solitons in coupled asymmetric quantum wells via interband transitions[J]. Physical Review B, 2009, 80(23): 235408.

[36] Gedalin M, Scott T C, Band Y B. Optical solitary waves in the higher order nonlinear Schrödinger equation[J]. Physical Review Letters, 1997, 78(3): 448-451.

[37] Hang C, Huang G X, Deng L. Generalized nonlinear Schrödinger equation and ultraslow optical solitons in a cold four-state atomic system[J]. Physical Review E, 2006, 73(3): 036607.

[38] 杜英杰, 杨战营, 白晋涛. 电磁感应透明介质的高阶非线性特性[J]. 光学学报, 2014, 34(6): 0627001.
Du Y J, Yang Z Y, Bai J T. High order nonlinear characteristics for electromagnetically induced transparency media[J]. Acta Optica Sinica, 2014, 34(6): 0627001.

[39] 任波, 余彦超, 徐小凤, 等. 高阶效应下对称三量子点系统中光孤子稳定性研究[J]. 物理学报, 2021, 70(22): 224205.
Ren B, She Y C, Xu X F, et al. Stability of optical soliton in symmetrical three-quantum-dot system under high-order effects [J]. Acta Physica Sinica, 2021, 70(22): 224205.

[40] Tang H, Wang D L, She Y C, et al. Dynamical analysis of temporal soliton with high order effects and cross-coupling relaxation of longitudinal optical phonons in double quantum wells[J]. The European Physical Journal D, 2016, 70(1): 22-29.

[41] Roskos H G, Nuss M C, Shah J, et al. Coherent submillimeter-wave emission from charge oscillations in a double-well potential [J]. Physical Review Letters, 1992, 68(14): 2216-2219.

[42] Pötz W. Coherent control of light absorption and carrier dynamics in semiconductor nanostructures[J]. Physical Review Letters, 1997, 79(17): 3262-3265.

[43] Hao X Y, Liu J B, Lü X Y, et al. Ultraslow optical solitons in a coupled double quantum-well nanostructure[J]. Communications in Theoretical Physics, 2009, 51(3): 519-523.

[44] Luo X Q, Wang D L, Zhang Z Q, et al. Nonlinear optical behavior of a four-level quantum well with coupled relaxation of optical and longitudinal phonons[J]. Physical Review A, 2011, 84(3): 033803.

[45] Nie Z Q, Zheng H B, Li P Z, et al. Interacting multiwave mixing in a five-level atomic system[J]. Physical Review A, 2008, 77(6): 063829.

[46] Li P Y, Zheng H B, Zhang Y Q, et al. Controlling the transition of bright and dark states via scanning dressing field[J]. Optical Materials, 2013, 35(5): 1062-1070.

[47] Fleischhauer M, Imamoglu A, Marangos J P. Electromagnetically induced transparency: optics in coherent media[J]. Reviews of Modern Physics, 2005, 77(2): 633-673.

[48] Neogi A. Transient interband light modulation via intersubband coupling light in undoped semiconductor quantum wells[J]. Optics Communications, 1997, 133(1/2/3/4/5/6): 479-486.

[49] Neogi A, Yoshida H, Mozume T, et al. Enhancement of interband optical nonlinearity by manipulation of intersubband transitions in an undoped semiconductor quantum well[J]. Optics Communications, 1999, 159(4/5/6): 225-229.

[50] Xue Y, Su X M, Wang G, et al. Photon switch in a quantum well by quantum interference in interband transitions[J]. Optics Communications, 2005, 249(1/2/3): 231-237.

[51] Wang Z G, Zheng Z R, Yu J H. Transient gain property of a weak probe field in an asymmetric semiconductor coupled double quantum well structure[J]. Physics Letters A, 2007, 370(2): 113-118.

# Storage and Retrieval of Optical Soliton in N-Type Quantum Well EIT Medium Under High-Order Effects

Hu Mingjun[1], Wang Denglong[1*], Dong Yaoyong[1,2], Ding Jianwen[1]

[1]*School of Physics and Optoelectronics, Xiangtan University, Xiangtan* 411105, *Hunan, China*;

[2]*School of Electromechanical Engineering, Guangdong University of Technology, Guangzhou* 510006, *Guangdong, China*

## Abstract

**Objective** As soliton can travel over long distance without attenuation and shape change due to the interplay balance between dispersion and nonlinearity in nonlinear media, it becomes a good information carrier in quantum information processing and transmission. Till now, the research on the storage and retrieval of optical soliton mainly focuses on ultra-cold atomic electromagnetic induction transparency (EIT) media. This is mainly because ultra-cold atomic systems can generate strong nonlinear effects under low light excitation. However, for practical applications, it is a great challenge to accurately control the optical soliton storage in the atomic EIT media due to the low temperature approaching to absolute zero and rarefaction. Fortunately, with the mature semiconductor quantum production technology, quantum wells have extensive application prospect in quantum information processing and transmission. Thus, we study the storage and retrieval of optical soliton in the GaAs/AlGaAs double quantum well EIT system.

**Methods** Based on the current experiments, we first propose an N-type four-level asymmetrical semiconductor GaAs/AlGaAs double quantum well EIT model. Subsequently, the interaction properties between the optical field and

semiconductor quantum wells in the system are studied by a semi-classical theory. The physical properties of the optical field are described by the Maxwell equation, while the semiconductor quantum well is described by the Bloch equation of quantum mechanics. Therefore, the Maxwell-Bloch (M-B) equations which govern the linear absorption and nonlinear propagating properties of the system are obtained. Generally, the analytic solution of the M-B equations cannot be obtained directly. Thereby, M-B equations are solved approximately by adopting a multiple-scale method. Correspondingly, the soliton solution [Eq. (63)] is chosen as the initial condition, and the M-B equations are numerically simulated by the Runge-Kutta method to explore the storage and retrieval of the probe pulse.

**Results and Discussions** Through the above methods, when the second control field is turned off, the linear absorption curve of the system exhibits a Lorentz absorption peak whatever the first control field changes [Fig. 2 (a)]. Fig. 2 (b) shows that when the second control field is only turned on, which means that the first control field is turned off, there is a single transparent window, and the width of the single transparent window becomes wider with the increasing strength of the second control field. When both the control fields are turned on, the double transparent window will occur, and the width of the double transparent windows is wider with the rising strength of any control field [Fig. 2 (c)]. Interestingly, after both the control fields are turned on, the double EIT windows show symmetrical distribution regardless of whether the strengths of the two control fields are equal or not [Fig. 2 (c)]. For the nonlinear case, Fig. 3 shows that with the low-order effect being considered, the optical soliton cannot propagate stably over a long distance with attenuation. The soliton instability is from the high-order dispersion of the system. After the high-order effects are only considered, the formed optical soliton can propagate stably over long distances (Fig. 4). Furthermore, Fig. 5 indicates that the optical soliton can be stored and retrieved by switching off and on the control fields, and the storage and retrieval fidelity of the optical soliton is higher than that of the ordinary optical pulse. Moreover, the amplitude of the stored optical soliton can be modulated by the strength of the control field. Specifically, when only the second control field is turned on, the amplitude of the stored optical soliton increases with the rising strength of the second control field [Fig. 6 (a)]. When both the control fields are turned on, the amplitude of the stored optical soliton rises with the increasing strength of the second control field under the unchanged first control field. However, if the second control field keeps unchanged, the amplitude of the stored optical soliton decreases with the increasing strength of the first control field [Fig. 6 (b)].

**Conclusions** In this paper, we propose an N-type four-level asymmetrical semiconductor double quantum well EIT model. Subsequently, we obtain the M-B equations governing the linear and nonlinear properties of the system through the semi-classical theory combined with the multiple-scale method. When both the control fields are turned on, the linear absorption curve of the system exhibits double EIT windows. Interestingly, the double EIT windows show symmetrical distribution regardless of whether the strengths of the two control fields are equal or not. For the nonlinear case, only after the high-order effects are considered, the formed optical soliton can propagate stably over long distances, and the optical soliton can be stored and retrieved by switching off and on the control fields. Meanwhile, the amplitude of the stored optical soliton can be modulated by the strength of the control field. When the first control field keeps unchanged, the amplitude of the stored optical soliton increases with the rising strength of the second control field. However, the amplitude of the stored optical soliton decreases with the increasing strength of the first control field under the unchanged second control field. The results can improve the fidelity for the storage and retrieval of quantum information in semiconductor quantum well devices.

**Key words** nonlinear optics; storage and retrieval of optical soliton; electromagnetically induced transparency; semiconductor quantum well